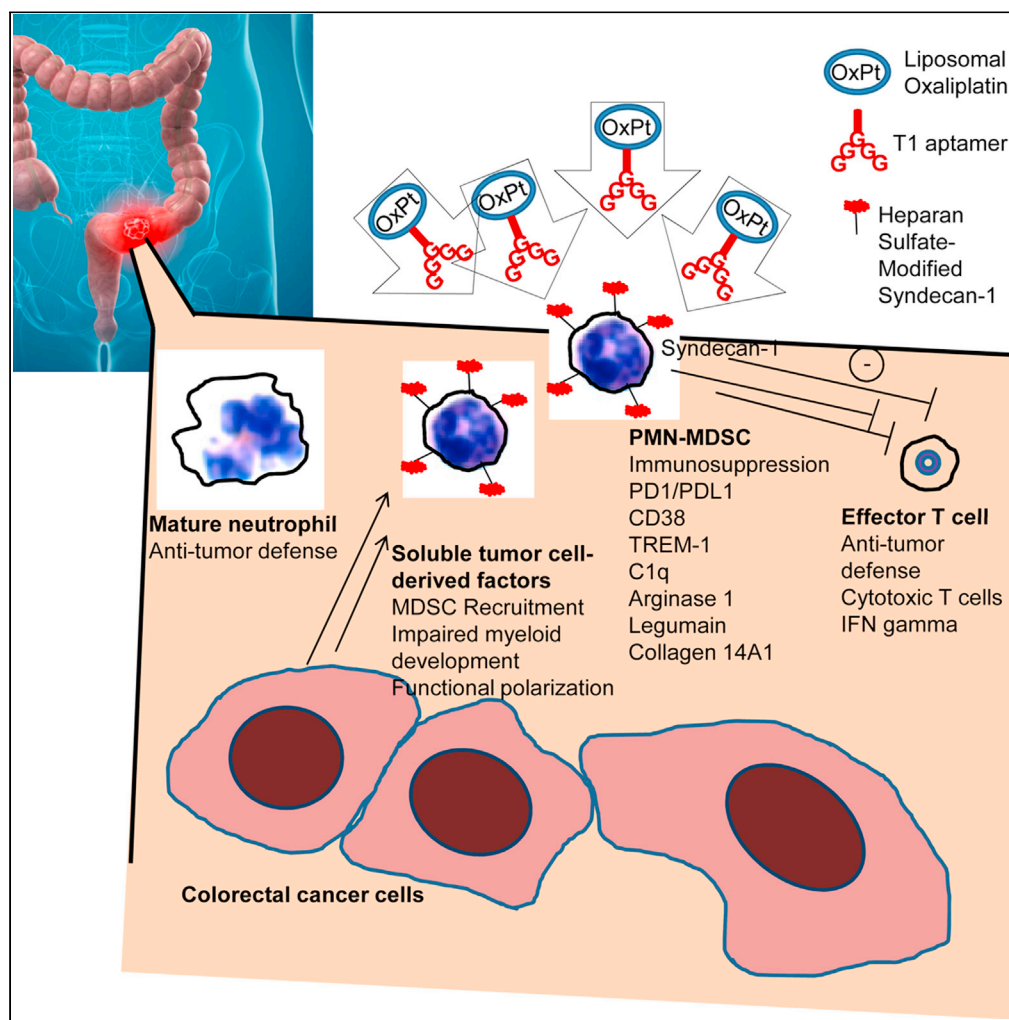


Article

# A heparan-sulfate-bearing syndecan-1 glycoform is a distinct surface marker for intra-tumoral myeloid-derived suppressor cells



Thomas Welte, Junhua Mai, Zhe Zhang, ..., Shu-shia Chen, Tian Wang, Haifa Shen

hshen@houstonmethodist.org

**Highlights**

Aptamer T1 binds to MDSCs in colorectal and pancreatic cancers with high specificity

This allowed intra-tumoral MDSC isolation for transcriptomic and functional analysis

T1-binding surface marker is composed of syndecan-1 on MDSC and K562 leukemia cells

Heparan sulfate on Syndecan-1 shapes the MDSC marker and is modulated inside tumors

Welte et al., iScience 24, 103349  
November 19, 2021 © 2021 The Author(s).  
<https://doi.org/10.1016/j.isci.2021.103349>



## Article

## A heparan-sulfate-bearing syndecan-1 glycoform is a distinct surface marker for intra-tumoral myeloid-derived suppressor cells

Thomas Welte,<sup>1</sup> Junhua Mai,<sup>1</sup> Zhe Zhang,<sup>1</sup> Shaohui Tian,<sup>1</sup> Guodong Zhang,<sup>1</sup> Yitian Xu,<sup>2</sup> Licheng Zhang,<sup>2</sup> Shu-shia Chen,<sup>2</sup> Tian Wang,<sup>3</sup> and Haifa Shen<sup>1,4,5,6,\*</sup>

## SUMMARY

**Myeloid-derived suppressor cells (MDSCs) infiltrate cancer tissue, promote tumor growth, and are associated with resistance to cancer therapies. However, there is no practical approach available to distinguish MDSCs from mature counterparts inside tumors. Here, we show that a recently isolated thioaptamer probe (T1) binds to MDSC subsets in colorectal and pancreatic tumors with high specificity. Whole transcriptome and functional analysis revealed that T1-binding cells contain polymorphonuclear (PMN)-MDSCs characterized by several immunosuppression pathways, ROS production, and T cell suppression activity, whereas T1-non-binding PMNs were mature and nonsuppressive. We identified syndecan-1 as the T1-interacting protein on MDSCs and chronic myelogenous leukemia K562 cell line. Heparan sulfate chains were essential in T1-binding. Inside tumors PMN-MDSCs expressed heparan sulfate biogenesis enzymes at higher levels. Tumor-cell-derived soluble factor(s) enhanced MDSCs' affinity for T1. Overall, we uncovered heparan-sulfate-dependent MDSC modulation in the tumor microenvironment and identified T1 as tool preferentially targeting tumor-promoting myeloid cell subsets.**

## INTRODUCTION

Myeloid-derived suppressor cells (MDSCs) are a key component of the tumor microenvironment, shaping this milieu via immunosuppressive activities, including impeding the accumulation and function of tumor-fighting cells such as cytotoxic CD8<sup>+</sup> T cells and NK cells (Gabrilovich et al., 2012). MDSCs also pose hurdles for cancer immunotherapy (Ostrand-Rosenberg and Fenselau, 2018). Advanced, reoccurring and drug-resistant cancers are often associated with massive increases of MDSCs and significant changes in the tumor microenvironment (Gonda et al., 2017; Weide et al., 2014). MDSCs include heterogeneous cell populations, which are mostly immature cell types (Almand et al., 2001). Based on cell surface markers and functional profiles, at least three subsets have been recognized, including polymorphonuclear (PMN-MDSCs), monocytic (M-MDSCs), and early stage (eMDSCs) (Bronte et al., 2016). PMN-MDSCs, most commonly found in cancer, resemble progenitors of neutrophils and express high levels of Ly6G in mice. M-MDSCs carry high levels of Ly6C and, unlike monocytes, barely express MHC II. A third subset at an earlier developmental stage was termed eMDSC (Bronte et al., 2016). MDSCs can also be grouped based on biological functions. For example, reactive oxygen species (ROS) production is high in PMN-MDSCs, whereas nitric oxide (NO) production is elevated in M-MDSCs (Gabrilovich et al., 2012).

The distinction between PMN-MDSCs and mature neutrophils is still under intense investigation. Certain features such as differences in gradient centrifugation, ER stress-related factor LOX-1, and GM-CSF-activated FATP2 have been shown to be associated with PMN-MDSCs. However, by themselves they may be insufficient for clearly separating PMN-MDSCs (Veglia et al., 2021). Other markers including Ly6G, Ly6C, and CD11b show only incremental differences in immature PMN-MDSCs relative to fully differentiated neutrophils. Furthermore, compared with peripheral sites, within tumors distinctive markers between MDSCs and mature anti-tumor myeloid subsets have not been established as well. This may in part be due to modulation and plasticity of myeloid cells. Upon entry into tumor site, M-MDSCs are capable to differentiate into tumor-associated macrophages (Tcyganov et al., 2018). A trans-differentiation of monocyte

<sup>1</sup>Department of Nanomedicine, Houston Methodist Academic Institute, Houston, TX 77030, USA

<sup>2</sup>Center for Immunotherapy Research, Houston Methodist Academic Institute, Houston, TX 77030, USA

<sup>3</sup>Department of Microbiology & Immunology, The University of Texas Medical Branch, 301 University Boulevard, Galveston, TX 77555, USA

<sup>4</sup>Innovative Therapeutic Program, Houston Methodist Cancer Center, Houston, TX 77030, USA

<sup>5</sup>Department of Cell and Developmental Biology, Weill Cornell Medicine, New York, NY 10065, USA

<sup>6</sup>Lead contact

\*Correspondence: [hshen@houstonmethodist.org](mailto:hshen@houstonmethodist.org)

<https://doi.org/10.1016/j.isci.2021.103349>



progenitors into PMN-MDSCs has also been reported (Mastio et al., 2019). Tumor-associated neutrophils show clear differences to splenic PMN-MDSCs based on their transcriptomes (Fridlender et al., 2012). Yet, immunosuppressive function—the defining feature of PMN-MDSCs—is a common attribute of tumor-associated neutrophils. Overall, there are still significant gaps in our knowledge of the markers and mechanisms that control MDSC formation and activity in tumors.

Despite these limitations, drug targeting tumor-promoting myeloid cells is a promising approach in cancer treatment (Cassetta and Pollard, 2018; De Henau et al., 2016; Elinav et al., 2013; Highfill et al., 2014; Kim et al., 2014; Welte et al., 2016). Directly suppressing myeloid cells or interfering with CXCR2-mediated MDSC migration alleviated resistance to immune checkpoint inhibitor treatment (Highfill et al., 2014; Kim et al., 2014). However, recent studies including single-cell sequencing analysis suggest that myeloid cells in the tumor microenvironment are a mixture of pro- and anti-tumor subtypes (Cassetta and Pollard, 2018; Lavin et al., 2017; Solito et al., 2014). Thus, ideal drugs will preferentially target the former subtypes.

Aptamers are short single-stranded nucleic acids that form sequence-specific secondary structures. They can selectively recognize specific protein domains or other molecular entities (Ellington and Szostak, 1990; Mi et al., 2010; Tuerk and Gold, 1990; Zhou and Rossi, 2017). In order to exploit this feature in cancer drug targeting, we screened a thiolated DNA aptamer library for sequences that could target components of tumors or metastatic microenvironment and identified a thioaptamer (T1) that was highly enriched in tumor tissue (Liu et al., 2018; Mai et al., 2018). The aptamer bound to PMN-MDSCs with highest affinity and T1-conjugated liposomes carrying doxorubicin had superior tumor-inhibition effects. However, the receptor for T1 on its target cells, the mechanism that leads to targeting of pro-tumor cell types, and the functional and transcriptomic features of T1 target cells remained all unknown. In the current study, we addressed these questions and identified the cell surface protein syndecan-1 as target for T1 binding and heparan sulfate as an essential part of the T1-binding site. In addition, we noted that T1 binding is a feature that distinguishes intra-tumoral immunosuppressive myeloid cells from fully mature, anti-tumor neutrophils. Heparan-sulfate-modified syndecan-1 was modulated inside tumors toward greater affinity to the T1 probe, providing an intrinsic mechanism for high targeting specificity and sparing protective bystander cells from T1. Furthermore, whole-transcriptome and functional analysis of T1 binding intra-tumoral PMN-MDSCs showed that they dampen the anti-tumor immune response through multiple pathways.

## RESULTS

### Morphologic and transcriptomic characteristics of tumor-associated MDSCs in colorectal and pancreatic tumors

We previously identified a T1 thioaptamer that binds to MDSCs (Liu et al., 2018). Here we utilized this probe to separate T1 binding- and T1 nonbinding cells for systematic MDSC characterization. We employed an *in vitro* binding assay with Cy5-conjugated T1 (T1-Cy5) to investigate interaction between T1 thioaptamer and tumor cells. T1-binding cells were identified by flow cytometry through co-staining with cell surface markers. Cells from colon cancers (established with murine CT26 and MC38 colon tumor lines) and pancreatic cancer (established with murine KPC cells) were applied in the study. In all tumors, T1 preferentially bound to large subsets of the myeloid lineage ( $CD45^+CD11b^+$ , Figure S1, upper panels). By comparison, T1 displayed only low percentage of binding to nonmyeloid lineages ( $CD45^+CD11b^-$  cells (Figure S1, upper panels). We also compared cells from subcutaneous and orthotopic tumors that were inoculated with the same batch of tumor cells and found that T1-binding characteristics of tumor-infiltrating  $CD45^+$  cells were indistinguishable for each model (Figure S1, bottom panels). The results suggest that tumor cells were decisive in regulation of T1 binding.

Next, we focused on the  $Ly6G^+$  myeloid subset, which contains PMN-MDSCs, a predominant MDSC population in tumors. Using T1 binding as a defining property, we observed three populations: (1)  $CD45^+CD11b^+Ly6G^{high}T1^+$  (assigned as  $Ly6G^{high}T1p$ ), (2)  $CD45^+CD11b^+Ly6G^{high}T1^-$  (assigned as  $Ly6G^{high}T1n$ ), and (3)  $CD45^+CD11b^+Ly6G^{low}Ly6C^{low}T1^+$  (assigned as  $Ly6G^{low}T1p$ ) (Figure 1A top panel). These cells were isolated by FACS, and their cell morphology, gene expression profile, and functional activities were investigated. Cytogenetic analysis showed that the T1-binding fraction of  $Ly6G^{high}$  cells was not fully mature with frequent presence of “band-shape” nuclei, whereas the nonbinding fraction was apparently more differentiated containing multi-lobed nuclei typical for mature neutrophils (Figure 1A bottom panels). In RNA sequencing analysis a group of genes previously established as PMN-MDSC markers were highly expressed in T1-binding  $Ly6G^{high}T1p$  cells compared with T1 nonbinding  $Ly6G^{high}T1n$  subset (Figure 1B). In particular, the subunits

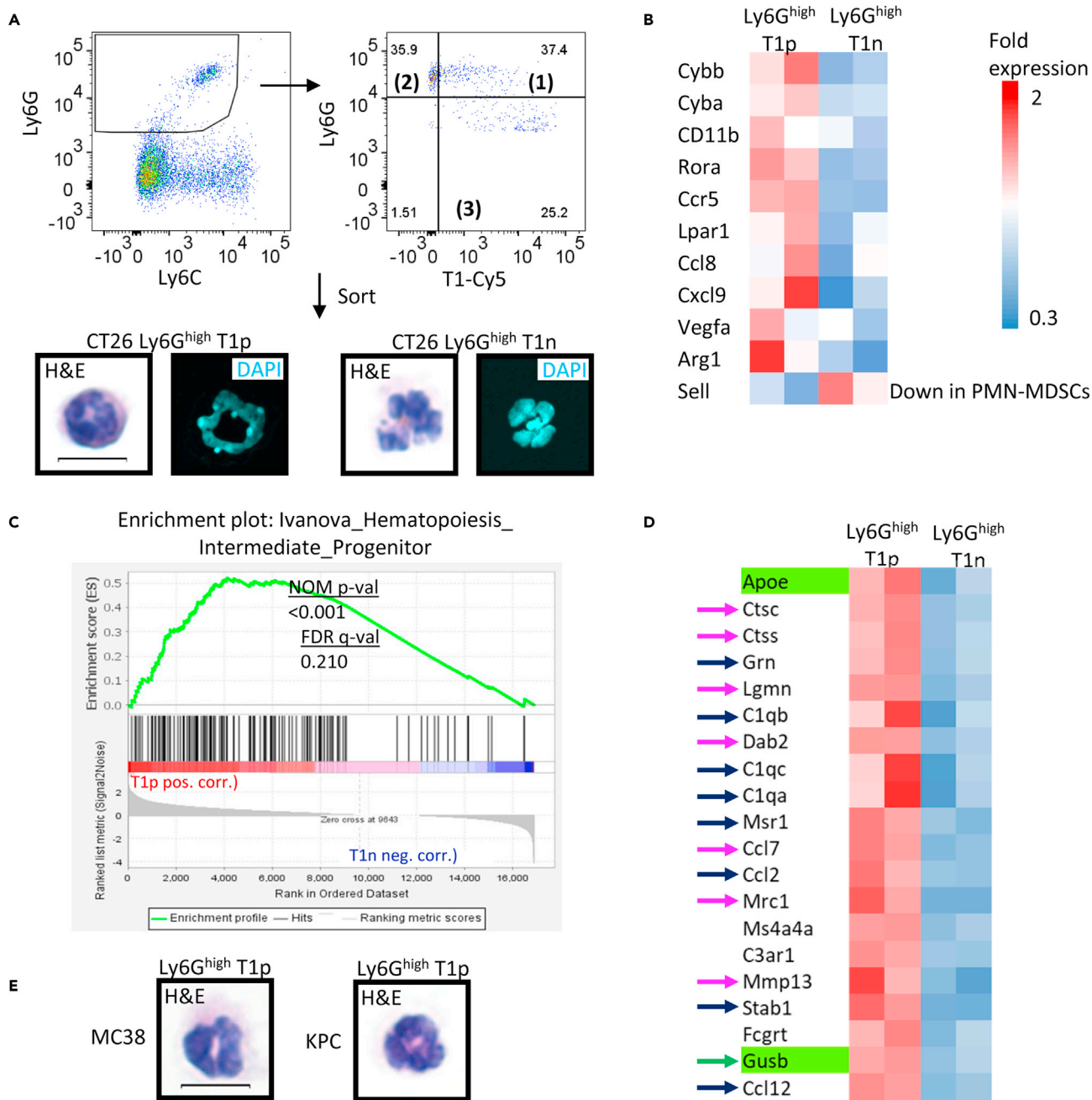


**Figure 1. Intratumoral, T1 thioaptamer binding PMNs display immature myeloid cell features and enhanced expression of genes in immunosuppression pathways**

(A) T1 binding and nonbinding populations were identified in CT26 tumors by FACS revealing three cell subsets based on the following criteria: (1) CD45<sup>+</sup>CD11b<sup>+</sup>Ly6G<sup>high</sup> T1 binding (assigned Ly6G<sup>high</sup>T1p), (2) CD45<sup>+</sup>CD11b<sup>+</sup>Ly6G<sup>high</sup> T1 nonbinding (assigned Ly6G<sup>high</sup>T1n), and (3) CD45<sup>+</sup>CD11b<sup>+</sup>Ly6G<sup>low</sup>Ly6C<sup>low</sup> T1 binding (assigned Ly6G<sup>low</sup>T1p). The three populations were separated by FACS sorting. Lower panels: (Left) H&E and DAPI staining of Ly6G<sup>high</sup>T1p; (right) Ly6G<sup>high</sup>T1n. H&E and DAPI pictures are from two different individual cells of same indicated group. All panels: 100x.

(B) RNA seq. transcriptomic comparison of Ly6G<sup>high</sup>T1p and Ly6G<sup>high</sup>T1n.

(C) Ly6G<sup>high</sup>T1p and Ly6G<sup>high</sup>T1n were subjected to gene set enrichment analysis (GSEA) with datasets related to hematopoietic development. Results were accepted at NOM p < 0.05, FDR q < 0.25.

(D) Genes with higher expression in Ly6G<sup>high</sup>T1p were ranked based on expression level; top 20 genes are shown. Pink arrows: previous evidence for involvement in immunosuppression function of myeloid cells. Dark blue arrows: involvement in T cell inhibition. Green arrows: anti-inflammatory.

(E) Same cell sorting as in A but with MC38 and KPC tumor-derived cells. Representative H&E staining of Ly6G<sup>high</sup>T1p cells is shown.

See also Figures S1–S4.

of NOX2 (also known as Cyba and Cybb), important players in ROS production and prototypic markers of PMN-MDSCs, were also expressed higher in Ly6G<sup>high</sup>T1p cells compared with Ly6G<sup>high</sup>T1n cells. Previous studies have shown that MDSCs and immunosuppressive regulatory dendritic cells are characteristically immature. By GSEA, we noticed an overlap in gene expression of Ly6G<sup>high</sup>T1p with a previously published hematopoietic progenitor population (Figure 1C), and myeloid-progenitor-associated markers ApoE and Gusb were expressed at a higher level in these cells (green highlights in Figure 1D). These results corroborate the cellular and molecular findings of immature status of Ly6G<sup>high</sup>T1p cells.

The transcriptomes of Ly6G<sup>high</sup>T1p and Ly6G<sup>high</sup>T1n cells were also analyzed for immunoregulatory gene expression. The top 50 genes significantly upregulated in T1-binding cells were arranged based on their expression levels (Figures 1D and S2). Remarkably, at least 32 of the top 50 genes have been previously linked to immunosuppression/anti-inflammatory function through different pathways (indicated by arrows next to the respective genes, Figures 1D and S2). Some genes have been associated with synergistically dampening immune response with PD-L1/PD-1 checkpoint axis (Trem2 [Molgora et al., 2020], Merck and Gas6 [Holtzhausen et al., 2019; Lee-Sherick et al., 2018], CD38 [Chen et al., 2018], C1q [Roumenina et al., 2019a, 2019b]); regulatory T cell recruitment/induction (CCL12, CCL2 [Kudo-Saito et al., 2013], progranulin [Kwack and Lee, 2017]); extracellular matrix remodeling/angiogenesis (Dab2 [Marigo et al., 2020], legumain [Shen et al., 2016]); dysfunction in antigen presentation (Msr1 [Herber et al., 2010]); and direct roles in myeloid cell polarization/differentiation toward MDSC (Lifr [Won et al., 2017], CCL2 [Chun et al., 2015], cathepsin S [Yang et al., 2014]). These findings support the notions that a T1-targeted myeloid subset in the tumor expresses immunosuppression-related genes at a higher level than the T1 nonbinding cells of a similar lineage and may be involved in several suppression pathways. We extended the MDSC separation studies to other colorectal (MC38) and pancreatic (KPC) tumors and found that in these models Ly6G<sup>high</sup>T1p cells are enriched for immature cells with band-shaped nuclei as well (Figure 1E).

The third cell subset of this study, the T1-binding Ly6G<sup>low</sup>T1p cells, was also submitted to [transcriptomic analysis](#). They were distinguished as a separate cell type in principal component analysis and tree/heatmap (Figure S3A). They displayed a similarity to hematopoiesis early progenitors (by GSEA, Figure S3C) and expressed the early hematopoietic development-marker CD34 (green highlight in heatmap of Figure S3C). Therefore, we concluded that this population is at an even earlier developmental stage than the Ly6G<sup>high</sup>T1p subset.

### T1 thioaptamer-binding cells display pro-tumor activities, such as ROS production, suppression of T cell activation, and induction of T cell exhaustion

MDSCs regulate immune responses through multiple mechanisms. We wished to discern the pathways prevalent in intra-tumoral T1-binding myeloid subsets. ROS production is a characteristic feature for MDSC subsets. More than 85% of T1-binding myeloid cells produced ROS in all three tumor models (Figure 2A).

To directly test MDSC-effects on T cell activation, we carried out *in vitro* T cell suppression assays with specific antigen (ovalbumin-peptide)-stimulated T cells as described earlier (Nagaraj et al., 2010; Sinha et al., 2012). In order to match their respective genetic background, we applied T cells of TCR-transgenic DO11.10 mice for studies of CT26-tumor-derived MDSCs, and T cells of TCR-transgenic OT1 mice for MC38 tumor-associated MDSCs. T cells were labeled with CFSE to follow their proliferation status and co-cultured with Ly6G<sup>high</sup>T1p and Ly6G<sup>high</sup>T1n populations isolated from tumors, and suppressive activity was measured. Ly6G<sup>high</sup>T1p cells diminished formation of IFN $\gamma$ <sup>+</sup> T cells (ELISPOT assay, Figure 2B). In addition, Ly6G<sup>high</sup>T1n cells did not show any detectable suppressive activity on the T cells (Figure 2B). The total number of T cells at end of co-culture with Ly6G<sup>high</sup>T1p was diminished more significantly in the CT26 model than in MC38 model (Figure 2C). This bears a similarity with findings in previous reports on MDSC functional evaluation (Nagaraj et al., 2010; Sinha et al., 2012). Furthermore, tumor-derived Ly6G<sup>high</sup>T1p cells had increased propensity to induce PD1 in nonproliferating (CFSE<sup>high</sup>) compartment of T cells, supporting a role in the induction of "exhausted" T cell phenotype (Figure 2D). PD1 ligand PD-L1 was expressed at a higher level in Ly6G<sup>high</sup>T1p cells compared with Ly6G<sup>high</sup>T1n (Figure 2E). Taken together, the immature MDSCs can be separated from mature myeloid cells based on their T1-binding property, and tumor-derived MDSCs are more immunosuppressive than their T1 nonbinding PMN counterparts.

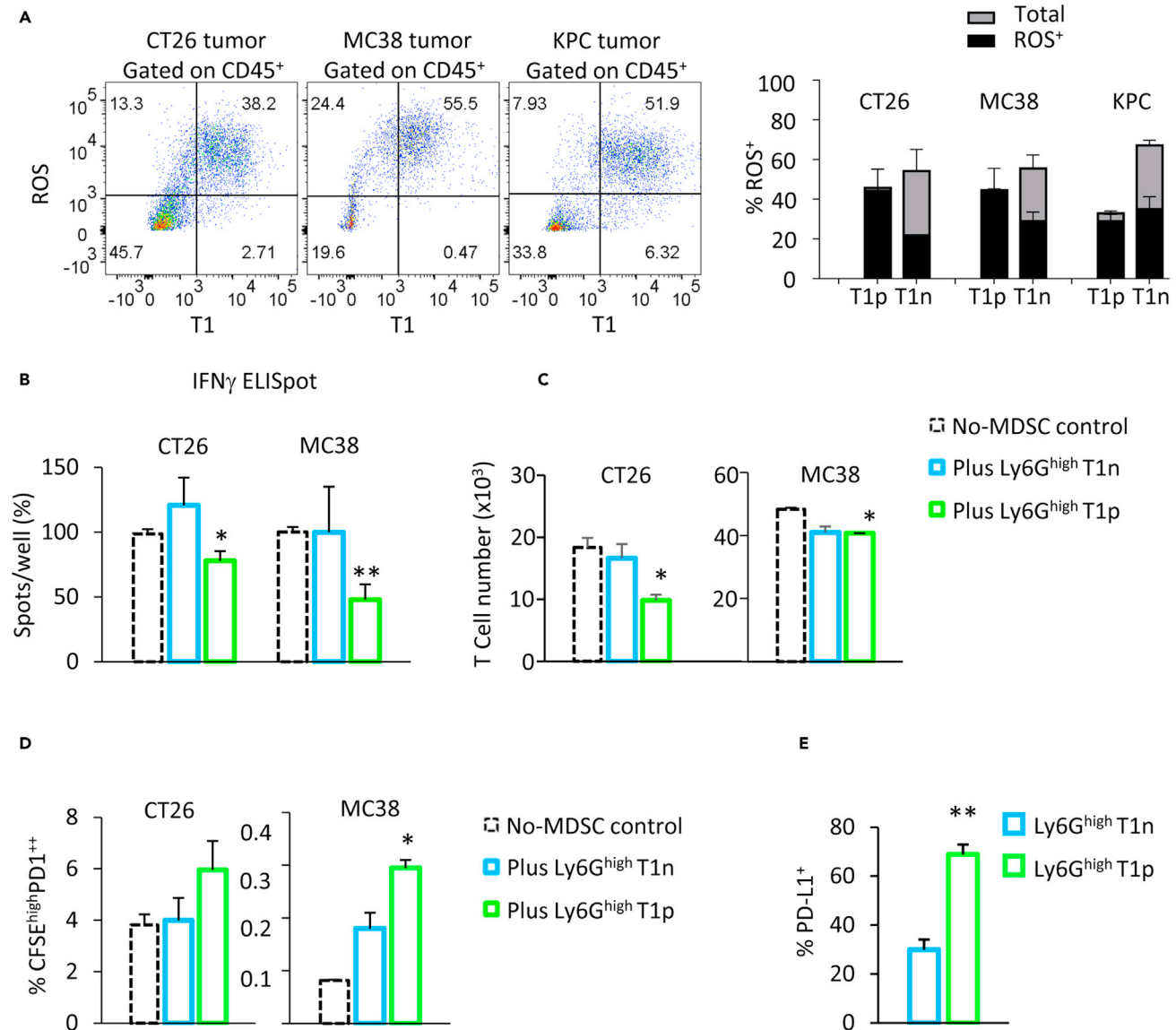


**Figure 2. T1 thioaptamer-target cells produce high levels of ROS and have immunosuppressive effects on T cells**

(A) Detection of ROS by flow cytometry. CT26, MC38, and KPC tumors were dissociated and treated with ROS detector (Cell ROX) for 30 min at 37°C, followed by staining with anti-CD45 to identify leukocytes, and T1 binding assay. Bar graphs (panel on the right) show percentage of ROS-producing cells in T1-binding (T1p) and T1 nonbinding (T1n) cells, respectively; n = 2–4 per group. Data are presented as mean  $\pm$  standard error.

(B–D) T cell suppression and exhaustion after co-culture with tumor-derived T1-binding PMN-MDSCs. Ly6G<sup>high</sup>T1p and Ly6G<sup>high</sup>T1n cells were isolated from indicated tumors and co-cultured with antigen-stimulated, OVA peptide-specific T cells. (B and C) T cell activation was followed by ELISpot assay for IFN $\gamma$ <sup>+</sup> T cells (B) and T cell number quantification at the end of co-culture period (C). (D) Exhausted T-cells were enumerated based on high expression of PD1 on nonproliferating (CFSE-high) cells. Bar graph shows group average of percentage of CFSE<sup>high</sup>PD1<sup>++</sup> (exhausted T cells) among total T cell population with standard error. Black bar: no MDSC control; blue bar: coculture with Ly6G<sup>high</sup>T1n; green bar: coculture with Ly6G<sup>high</sup>T1p. Representative results of three experiments are shown; \*p < 0.05, \*\*p < 0.01.

(E) High expression of PD-L1 in CT26-tumor-associated T1-binding PMNs (Ly6G<sup>high</sup>T1p) relative to T1 nonbinding PMN subset, by CYTOF. n = 3, \*\*p < 0.01.

### Syndecan-1 mediates T1 binding to immature myeloid cells

Using GSEA analysis we detected similarity between the T1-binding subsets Ly6G<sup>high</sup>T1p and Ly6G<sup>low</sup>T1p cells inside solid tumors and subsets of acute and chronic myeloid leukemia (Figure S4, Table 1). Accordingly, we found that T1 specifically bound to the immortalized human CML cell-line K562 in a dose-dependent manner (Figure 3A).

**Table 1. Similarity of intra-tumoral T1 binding myeloid cells with CML and AML<sup>a</sup>**

Cell subset	Gene set	NOM p-val	FDR q-val
Ly6G <sup>high</sup> T1p	VALK AML Cluster 5	0.006	0.011
Ly6G <sup>high</sup> T1p	VALK AML Cluster 11	0.002	0.012
Ly6G <sup>high</sup> T1p	VALK AML Cluster 13	0.007	0.011
Ly6G <sup>high</sup> T1p	VALK AML with MLL Fusion	0.007	0.011
Ly6G <sup>low</sup> T1p	VALK AML Cluster 10	0.021	0.070
Ly6G <sup>low</sup> T1p	GRAHAM_CML_DIV._VS._NORM._QUIESC._UP	<0.001	0.003

<sup>a</sup>Transcriptomes of Ly6G<sup>high</sup>T1p, Ly6G<sup>low</sup>T1p and Ly6G<sup>high</sup>T1n cells were subjected to gene set enrichment analysis (GSEA) with datasets related to leukemia. Results were accepted at NOM  $p < 0.05$ , FDR  $q < 0.25$ .

In order to molecularly identify the biomarker recognized by T1, we applied K562 cells as a reagent and determined the T1-binding partner on their cell surface. To that end, T1 was modified with an ABAL moiety, which allowed covalent UV cross-linking to the nearby interaction partner via phenyl-azide residue, as well as streptavidin column purification of T1-ABAL:protein complexes via biotin residue (Vinkenberg et al., 2012) (Figures 3B and S5). Subsequently, T1-ABAL-binding cell surface proteins were identified by mass spectrometry. Syndecan-1 was revealed as prime candidate T1-binding protein (Figure 3B). In a transcriptomic study, *SDC1* encoding syndecan-1 was expressed at higher level (5.75fold increase) in the T1-binding fraction of K562 cells (T1pK562) than the nonbinding fraction (T1nK562) (Figure 3C), pointing again to syndecan-1 as candidate for T1 binding. Syndecan-1 is highly expressed on the surface of K562 cells (Figure 3D). Confocal microscopy detected overlap of T1 and syndecan-1 on the cell surface (Figure S6A). To verify the finding, we took a CRISPR-based approach to generate *SDC1* knockout (KO) cells. In contrast to parental K562 cells, *SDC1* KO cells showed diminished T1 binding (Figures 3D–3F, S6B and S6C).

In tumor-infiltrating leukocytes, the syndecan-1<sup>+</sup> cell fraction showed much higher percentage of T1 binding compared with the whole leukocyte population, with up to 80%–98% T1 binding by syndecan-1<sup>+</sup> cells in tumors of CT26, MC38, and KPC (Figure 4A). For comparison, we also analyzed the syndecan-3<sup>+</sup> population in CT26 tumors. We performed tSNE analysis on the CD45<sup>+</sup> leukocytes combining myeloid lineage markers, syndecan-3, and T1-Cy5 thioaptamer binding. This revealed two very different patterns for the “spread” of syndecan-3 expression and T1-Cy5 binding within the cellular landscape of CD45<sup>+</sup> cells (Figure 4B). Thus, syndecan-3 and T1-binding are not directly correlated, in contrast to what is found with syndecan-1. These results support syndecan-1 as T1-binding partner on the cell-surface.

### T1 interacts with heparan sulfate side chains on syndecan-1

Syndecan-1 is a member of the proteoglycan protein family, carrying four chains of heparan sulfate and two chains of chondroitin sulfate on its extracellular domain as a result of posttranslational modifications. Previous studies have shown that heparan sulfate side chains are sites of interaction between syndecan-1 and extracellular factors such as chemokines (Bernfield et al., 1999; Li et al., 2002b; Pasqualon et al., 2016). Interestingly, soluble heparin was a strong competitor against T1 in binding to K562 cells even at the lowest concentration in a binding assay, suggesting that T1 had affinity to heparin/heparan sulfate (Figures 5A and S7A). In contrast, we did not observe an effect of heparin on binding of E-selectin thioaptamer (ESTA), a control aptamer that binds to cell surface E-selectin (Mai et al., 2018) at low to medium concentrations of heparin (Figure 5A). Chondroitin sulfate and hyaluronic acid, two other polysaccharides sharing a similarity with heparan sulfate, were also tested as competitors for T1 binding. However, these displayed only low affinity for T1 in comparison to heparin (Figure 5B). Other negatively charged polymers such as polyIC (pIC) could also compete against T1 binding at a moderate concentration (Figure S7B), suggesting that negative charge was relevant in T1 binding, although heparin was more efficient in the competition.

It has been reported that deficiency in the *EXT1* gene encoding exostosin 1, a key enzyme in mediating heparan sulfate polymerization, leads to inhibition of heparan sulfate synthesis (Ren et al., 2018). We applied CRISPR technology to knock out *EXT1* in K562 cells. Knockout of this gene dramatically diminished heparan sulfate on the cell surface, almost down to an undetectable level (Figures 5C and 5D). As a result, the *EXT1* KO cells were impaired in their ability to bind T1 compared with parental K562 (Figures 5E and 5F). Heparan sulfate cleavage can be carried out enzymatically with heparanases (Reiland et al., 2004).

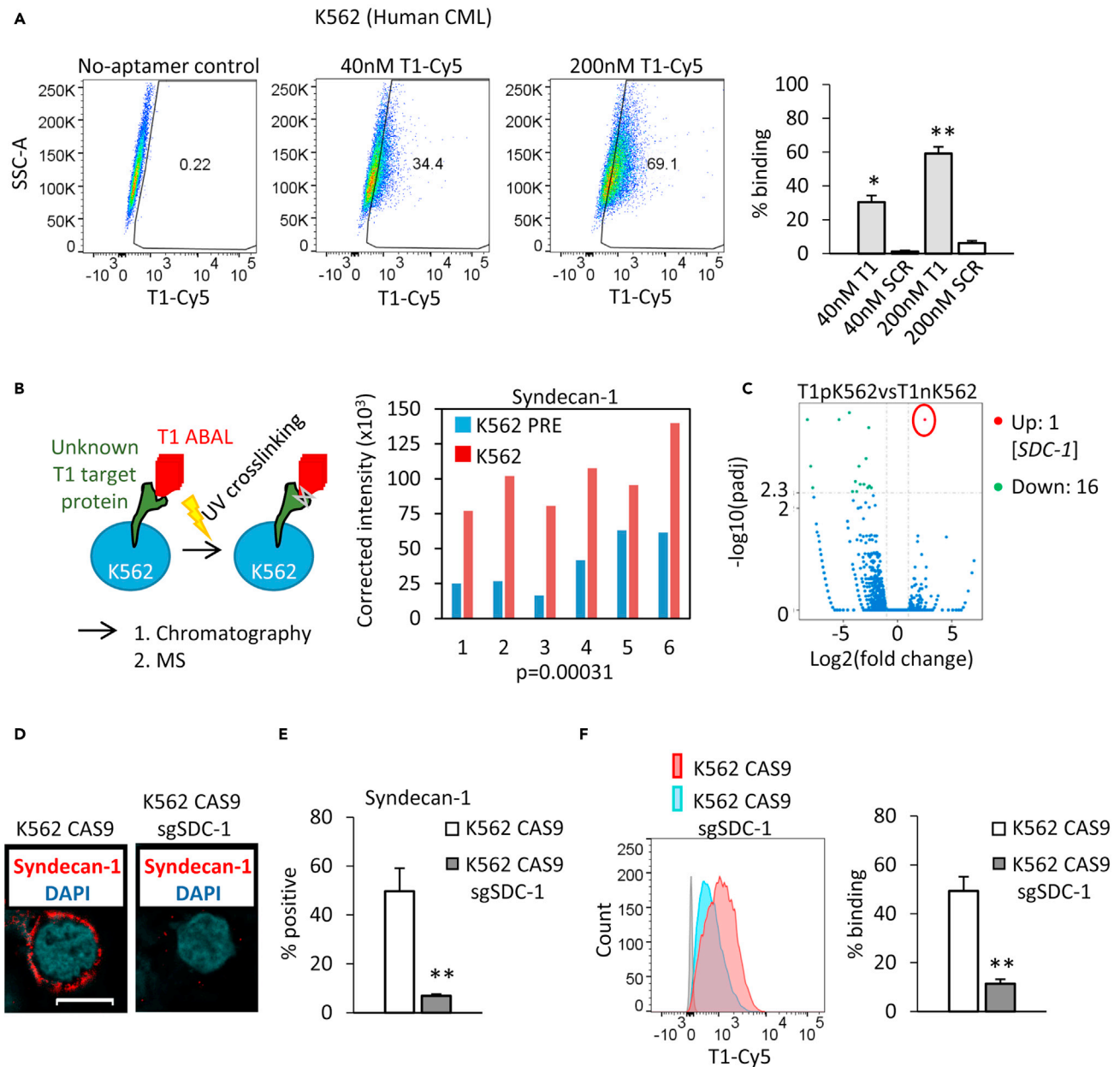


**Figure 3. T1 thioaptamer-binding protein on cell surface is syndecan-1, as identified by mass spectrometry and confirmed by CRISPR KO**

(A) Human K562 CML cells were evaluated for T1-binding. Cy5-labeled T1 (T1-Cy5) was compared with Cy5-labeled analogue with scrambled sequence (SCR-Cy5) as specificity control. \* $p < 0.05$  for percentage of binding of T1-Cy5 compared with SCR-Cy5.

(B) Schematic view on approach for T1-binding protein identification in K562 cells. ABAL-modified T1 (T1-ABAL) was used, allowing covalent UV cross-linking of the aptamer to putative protein binding partner (via phenyl azide) and column enrichment (via biotin) followed by mass spectrometric (MS) protein identification. Specificity control: same procedure but in presence of 50x excess of unmodified T1 (K562 PRE). Right panel: MS results identified syndecan-1 as candidate T1-binding partner. Graph shows quantities of syndecan-1 associated with T1-ABAL based on syndecan-1 peptide fragments detected by MS in samples (K562) relative to specificity control (K562 PRE).  $n = 6$  identical experimental repeats.  $p$  value for difference between sample and specificity control is shown.

(C) T1-binding (T1p) and T1 nonbinding (T1n) fractions of K562 cells were isolated by flow cytometric cell sorting and analyzed by RNA sequencing. Statistical significance for differential expression:  $p_{adj} < 0.05$ . Upregulated gene (*SDC-1*) is highlighted by red circle. (D–F) CRISPR knockout of *SDC1* in K562 cells. Parental K562 cells stably expressing CAS9 (K562 CAS9) and K562 CAS9 cells stably transduced with *SDC1* specific guide RNA (*SDC-1* KO line, K562 CAS9 sgSDC1) were compared in syndecan-1 expression and T1 binding.

(D) Representative confocal microscopy images of syndecan-1-stained cells (100x) are shown.

**Figure 3. Continued**

(E) Quantification of percentage of syndecan-1 expressing cells measured by FACS. Data are presented as means with standard errors; \*\*p < 0.01.

(F) Representative FACS plots of syndecan-1-stained cells subjected to T1-Cy5 binding assay are shown. Right panel: quantification of percentage of T1-binding cells. \*\*p < 0.01. n = 3 experimental repeats.

See also [Figures S5](#) and [S6](#).

Pretreatment of K562 cells with recombinant human heparanase 1 reduced T1 binding ([Figure 5G](#)). Similarly, pretreatment with bacterial heparinases I/III reduced heparan sulfate levels on K562 and PMN-MDSCs and resulted in reduced T1 binding ([Figure S8B](#)). Taken together, our data demonstrated the involvement of heparan sulfate chains in T1 binding. In addition, correlation study on the FACS data revealed that, within a cell-type, T1 binding increases with the amount of heparan sulfate present on cell surface ([Figure S8A](#)).

**Heparan sulfate biogenesis enzymes are upregulated in PMN-MDSC upon tumor-entry, and tumor-cell-derived soluble factors induce a higher T1 affinity on these cells**

Next, we isolated tumor-associated leukocytes of a CT26 tumor and performed the T1 binding assay in absence or presence of heparin competition. Heparin diminished T1 binding on target cells, thus replicating the results of leukemia cells in tumor-associated leukocytes and implicating that heparan sulfate is of general importance in T1 binding to target cells in tumors ([Figure 6A](#)). We hypothesized that heparan sulfate fine-structure could be a decisive factor in T1 binding. Besides sugar chain polymerization steps, enzymatic modifications such as desulfation/desulfation on specific O- and N-positions and sugar epimerization are intrinsic to heparan sulfate synthesis, creating the fine structure of heparan sulfate. We compared gene expression of the heparan sulfate synthesis/modification machinery in T1-binding and nonbinding cells and noted a specific subset of heparan sulfate biosynthesis/modification genes was expressed higher in T1 binding Ly6G<sup>high</sup>T1p subset compared with T1 nonbinding subset ([Figure 6B](#), [Table 2](#)). Several of these genes are expressed at a higher level in tumor-associated PMNs compared with PMN subsets outside of tumors (normal neutrophils and splenic PMN-MDSCs, [Figure 6C](#)). To test whether this may impact T1-binding, we analyzed T1-binding cells in different tissues of the same mouse. It was noted that CD11b<sup>+</sup>Ly6G<sup>high</sup> cells isolated from tumors had a higher percentage and greater mean fluorescence intensity (MFI) of T1 binding compared with counterparts in spleen and blood ([Figures 6D](#) and [S9A](#)). Analogous results were obtained when comparing the totality of CD11b<sup>+</sup> cells in tumor, spleen, and blood ([Figure S9B](#)). These findings suggested two nonexclusive possibilities: either cells with high T1-binding capacity were preferentially recruited to the tumor or tumor-microenvironment might foster and modify T1 binding of myeloid cells in their vicinity. We tested the latter possibility by co-culturing naive CD11b<sup>+</sup> bone marrow cells with tumor cells. Compared with bone marrow cells alone, co-cultures with CT26 or MC38 cells, respectively, contained a higher number of CD11b<sup>+</sup> cells at the end of culture period ([Figure S10](#)). Tumor cells also enhanced T1-Cy5 binding capacity as evident from increased MFI of T1-Cy5 in CD11b<sup>+</sup>Ly6G<sup>high</sup> cells ([Figure 6E](#)). To investigate the mechanism behind tumor-cell-induced T1 binding of myeloid cells, we co-cultured bone marrow cells and CT26 tumor cells in a trans-well format. Although bone marrow and CT26 cells were separated by a membrane in this setup, CT26 still enhanced binding of T1 aptamer to Ly6G<sup>+</sup> cells of the bone marrow ([Figures 6F](#) and [S11](#)). Similarly, treatment with CT26-tumor-cell-conditioned medium also led to enhanced T1 binding ([Figures 6F](#) and [S11](#)). Combined, these results suggest that soluble factor(s) derived from CT26 tumor cells could enhance T1 binding on myeloid cells. Overall, tumor cells are known to coopt myeloid cells and enhance their pathogenic functions. The aforementioned findings indicate this may entail tumor-cell-derived soluble factor(s) and transcriptional upregulation of heparan sulfate biosynthesis pathway.

**T1 thioaptamer-tagged, oxaliplatin-loaded liposomes are effective in tumor therapy**

To apply the unique affinity of T1 probe for intra-tumoral MDSCs and achieve enhanced targeting of MDSCs in colon cancer therapy, we coupled T1 to a cytotoxic drug, oxaliplatin. We incorporated T1 thioaptamer into oxaliplatin-loaded liposomes and utilized this regimen in therapy of CT26-tumor-bearing mice (T1-lipOXPt, [Figure S12](#)). This strategy efficiently reduced the numbers of T1-binding PMN-MDSCs present within tumors ([Figure S12A](#)). Although the drug treatment led to a decrease in T1-binding PMNs among tumor-infiltrating leukocytes, it did not affect T1 nonbinding PMNs ([Figure S12A](#)). This result supports that specific targeting of pro-tumor PMN-MDSCs by T1 thioaptamer is maintained *in vivo* when utilized in a liposomal drug. Even when starting treatments at relatively big tumor size (average tumor volume approximately 250 mm<sup>3</sup>), T1-lipOXPt significantly reduced tumor progression and was more efficient than free oxaliplatin at a moderate oxaliplatin dose (5 mg/kg, [Figure S12B](#)). By repeatedly applying

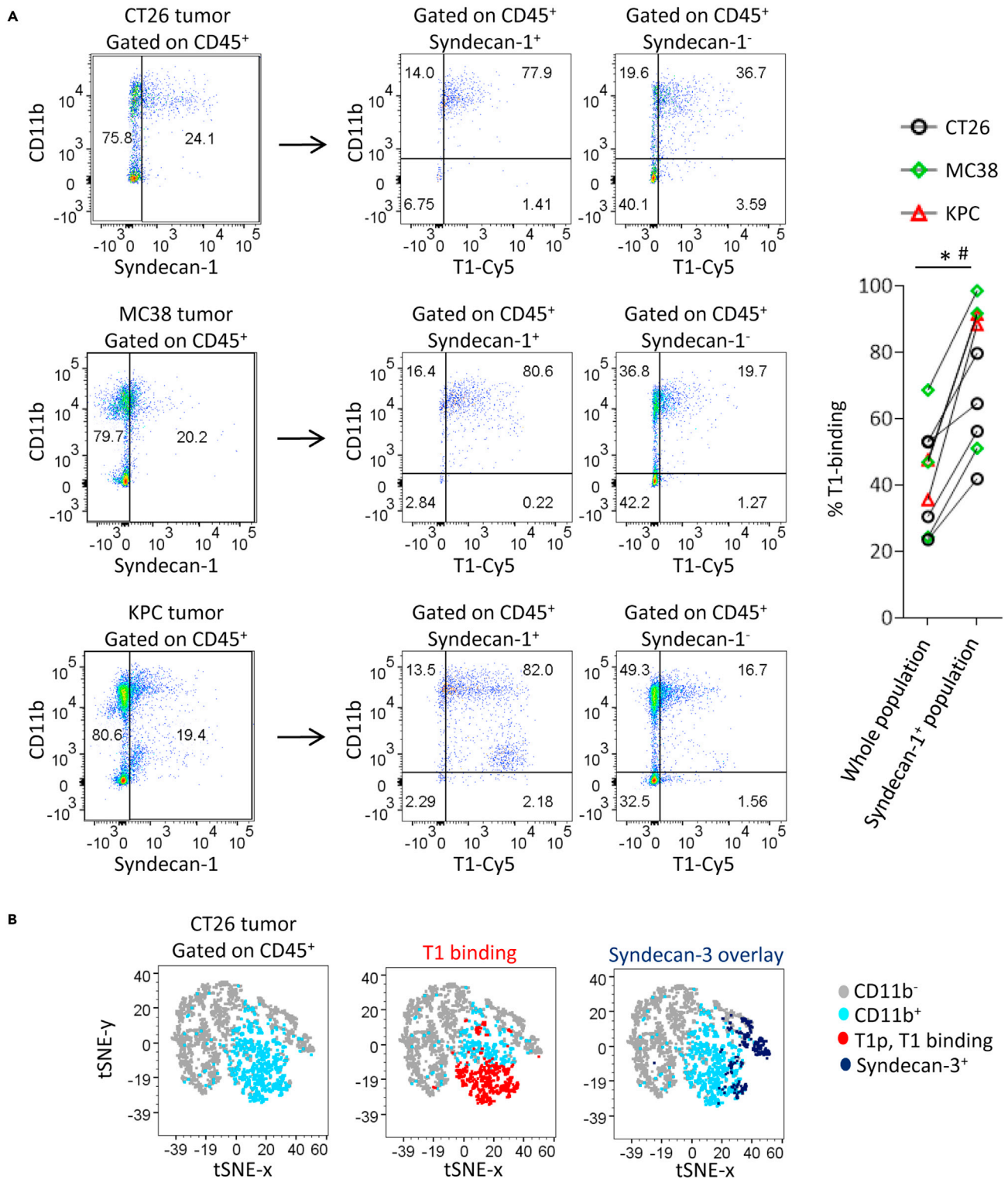


**Figure 4. Syndecan-1 expression and T1 thioaptamer binding are correlated in tumor-associated leukocytes**

Tumor-associated leukocytes from CT26, MC38, and KPC tumors were analyzed based on T1-binding and co-staining with CD45, CD11b, and syndecan-1 antibodies.

**Figure 4. Continued**

(A) FACS plots and graph depict T1 binding of syndecan-1<sup>+</sup> and syndecan-1<sup>-</sup> fractions, as well as whole leukocyte population. \*, #p < 0.05 for comparison between T1 binding in syndecan-1<sup>+</sup> fraction and whole leukocytes in CT26 model (\*) and MC38 model (#), respectively. n = 4 for CT26, n = 3 for MC38, and n = 2 for KPC.

(B) Another family member—syndecan-3 was examined for comparison and did not show correlation with T1 thioaptamer binding. CT26 tumor data were analyzed by tSNE. Individual cell subsets are assigned different colors in tSNE plots as determined based on markers expressed. T1 Cy5 binding is shown as red overlay (middle panel). Syndecan-3 expression is shown as dark blue overlay (right panel). Result is representative of two tumors analyzed.

T1-lipOXPt (5 mg/kg, three times per week for two weeks), durable drug efficacy in tumor inhibition was achieved even at later time points (Figure S12C). Feasibility of the latter approach of multiple treatments with T1-lipOXPt (5 mg/kg per treatment) was supported by the observation that such a regimen was well tolerated by the animals as assessed by the animals' body weight.

**DISCUSSION**

PMN-MDSC is an important pro-tumor player in the tumor microenvironment. Here we addressed several open questions regarding their mechanism of action and their therapeutic depletion to support tumor immunotherapies. (1) We used a PMN-MDSC targeting probe—T1 thioaptamer to isolate them from colorectal tumors for transcriptomic/functional analysis and determined the immunosuppression pathways present in these cells. (2) We further identified a syndecan-1 glycoform as a specific marker on the cell surface of PMN-MDSCs and (3) unraveled tumor-cell-dependent mechanisms that result in changes of the heparan sulfate biosynthesis machinery and upregulation of the syndecan-1 glycoform marker when the cells are inside tumors.

Transcriptome analysis revealed that 32 of the top 50 genes overexpressed in tumor-associated, T1-binding myeloid cells were genes associated with dampening immune response. The nature of these upregulated genes indicates that T1-binding myeloid cells suppress immune responses through multiple pathways. The *Col14A1* gene, a collagen family member, was also overexpressed in T1-binding myeloid cells. It was previously reported that collagen deposition promoted therapy resistance through T cell exhaustion, and *Col14A1* was upregulated in PD-L1-therapy-resistant lung tumors (Peng et al., 2020). Furthermore, the same T1-binding myeloid subsets are also efficient inducers of PD-1 expression, leading to the development of nonproliferating, PD-1-expressing T cells, a phenotype linked to T cell exhaustion (Ahmadzadeh et al., 2009; Barber et al., 2006; Day et al., 2006; Zhou et al., 2017). Thus, accumulation of T1-binding MDSCs will most likely lead to resistance to PD-L1/PD-1-based immunotherapies, and depletion of these cells provides an avenue for sensitizing treatment.

Our studies also suggest syndecan-1 as the target protein for T1 binding on tumor-associated MDSCs as well as the essential role of heparan sulfate in modulating T1:MDSC interaction. Previous studies have implicated syndecan-1 and other syndecan family members in immunoregulation. Interactions between syndecan-1 and extracellular factors either entirely or at least partially depend on its heparan sulfate chains (Bernfield et al., 1999; Pasqualon et al., 2016; Pinal et al., 2001; Zhang et al., 2013). Although syndecans are expressed in multiple cell types, the fine structure of heparan sulfate that is attached to the protein as a result of posttranslational modification may define binding specificity and function of the protein. A previous study showed that alterations in heparan sulfate contributed to the immature, pro-tumor state of DCs (El Ghazal et al., 2016). Deficiency of *Ndst1* (N-deacetylase/N-sulfotransferase), one of the enzymes in heparan sulfate biogenesis, promoted DC maturation and led to priming T cell immunity and tumor growth inhibition. In addition, knockout of the *Sdc4* gene led to DC maturation and diminished tumor growth, suggesting a role of syndecan-4 in immature DC function. Applying IL-10 treatment on human PBMCs, Heine et al. derived a monocyte population, which reduced DC-induced T cell proliferation, whereas adding a blocking antibody against syndecan-4 restored T cell expansion in these co-cultures, implicating a direct role of syndecan-4 in T cell suppression (Heine et al., 2017). An *ex vivo* study with lymphocytes of inflammatory and noninflammatory breast cancer patients co-cultured with syndecan-1-silenced tumor cell lines showed that depending on disease subtype, syndecan-1 knock-down promoted Th17 or Th1 cell expansion, suggesting an immunomodulatory role of syndecan-1 in T cell regulation (Saleh et al., 2019). These findings are reminiscent of an early study reporting that heparin, a competitor disrupting cellular interactions via heparan sulfate, could enhance T cell activation in mixed leukocyte reaction and anti-tumor cytotoxicity (Dziarski, 1989).

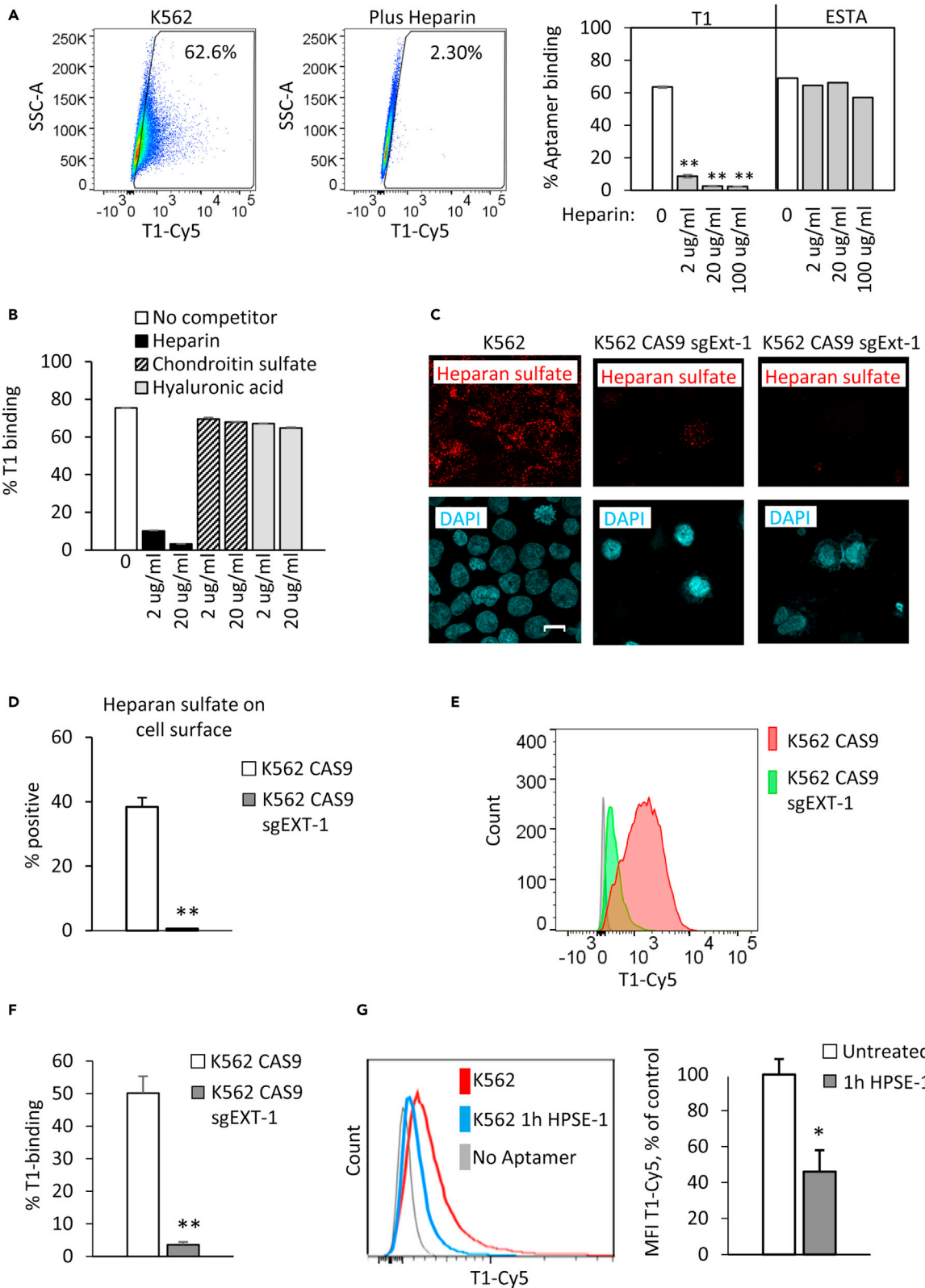


**Figure 5. Heparan sulfate is an essential part of T1 thioaptamer binding site**

(A) Competition of T1 binding to K562 cells by increasing concentrations of heparin (0–100 ug/mL). E-selectin thioaptamer (ESTA) served as a negative control in the assay. \*\*p < 0.001 relative to percentage of T1-Cy5 binding in absence of heparin. (B) Comparison of heparin, chondroitin sulfate, and hyaluronic acid in T1-binding competition assay. (C–F) CRISPR knockout of exostosin 1 in K562 cells. Parental K562 CAS9 cells were stably transduced with guide RNA for *EXT1* gene (*EXT1* KO, K562 CAS9 sgExt1). (C) Parental and *EXT1* KO cells were evaluated for presence of heparan sulfate by anti-heparan sulfate staining and confocal fluorescence microscopy. (D–F) Heparan sulfate levels on cell surface and T1-Cy5 binding were quantified by flow cytometry; \*\*p < 0.01 between parental and KO cell line. (G) K562 cells were treated with recombinant human heparanase I (HPSE I) for 1 h at 37°C, followed by T1 binding assay. Amount of T1 binding per cell was determined based on MFI of T1-Cy5 binding to cells. \*p < 0.05. See also [Figures S7](#) and [S8](#).

Increasing evidence suggest that heparan sulfate is an important (co-)receptor for binding of proinflammatory cytokines, chemokines, and growth factors (Kiefer et al., 1991; Pasqualon et al., 2016; van Gemst et al., 2018). Among them, macrophage migration inhibitory factor (MIF) is a cytokine binding to syndecan-1 via heparan sulfate (Pasqualon et al., 2016). MIF is involved in myeloid cell development. MIF secreted from 4T1 breast cancer cells is known to induce the “differentiation” of myeloid cells into MDSCs (Simpson et al., 2012). It’s also likely that T1-targeted, heparan-sulfate-modified syndecan-1 controls immature status of myeloid lineages and is directly involved in T cell suppression.

Mechanistically, we discovered through trans-well co-culture experiments that soluble CT26-tumor-cell-derived factor(s) are capable to induce the syndecan-1 glycoform marker on myeloid cells. Corroborating the finding, CT26-tumor-cell-conditioned medium had the same effect. Such changes occurred without alteration of the syndecan-1 protein level, supporting the role of posttranslational syndecan-1 modification (TW unpublished). Heparan sulfate is a variable part of syndecan-1 and is subject to different modulation mechanisms. We detected higher expression levels from genes encoding heparan sulfate biosynthesis/modification enzymes in PMN-MDSCs compared with nonsuppressive PMNs, indicating their potential relevance in establishing the syndecan-1 glycoform marker. Multiple mechanisms may be responsible for the differential expression (Suhovskih et al., 2014; Swart and Troeberg, 2019). Tumor cell-derived cytokines may induce the expression of these genes. Alternatively, tumor-derived extracellular factors such as heparanases (Escobar Galvis et al., 2007), sulfatases (Dhanasekaran et al., 2015; Hossain et al., 2010), and hypoxia (Khurana et al., 2012; Li et al., 2002a) may directly modify heparan sulfate structure, thereby modulating affinity to T1.

Aptamers can interact not only with proteins but also with sugar moieties such as those present in heparan sulfate. Previous studies indicated that positive charges on guanines of an aptamer and negatively charged residues in the sugar back bone contributed to the interaction (McRae et al., 2017). Indeed, there is a guanine-rich region within T1. Future studies should explore the role of such structural features in binding affinity and specificity. Due to the wide-spread physiologic importance of cell surface glycoproteins, approaches have been developed to derive aptamers against them (Ma et al., 2018). We speculate that aptamer-sugar chain contact is a common mechanism in these scenarios. In this study, confocal fluorescence microscopy results suggest T1-binding sites overlap with syndecan-1 location on the cell surface. In addition, we found that T1-binding sites on syndecan-1 are distinctly distributed during cellular processes such as cell-cycle progression (Figure S6A). Thus, although the disaccharide unit sequences of heparan sulfate chains have not yet been identified due to the lack of available experimental tools (Kurup et al., 2007; van den Born et al., 2005), T1 aptamer may serve as a novel tool for detection of heparan-sulfate-associated biological molecules and cellular events.

Our studies have also shown that T1 recognizes chronic myelogenous leukemia (CML) line K562. In addition, GSEA study revealed similarity of T1-binding tumor-infiltrating cells with several types of AML and CML. Similar as in MDSCs, blockage of differentiation is a hallmark feature of AML and CML (Chang et al., 2007; Chopra and Bohlander, 2019; Rosenbauer and Tenen, 2007; Terstappen et al., 1992). These results further support that T1-binding capability is a characteristic feature of myeloid cells at an immature developmental stage. MDSC marker expression and immunosuppression by the transformed clone itself has been reported in myeloid leukemias (Christiansson et al., 2013; Giallongo et al., 2014; Pyzer et al., 2017). Despite of differences in autonomous growth and stem cell potential, myeloid leukemias and the T1-binding tumor-infiltrating myeloid cells/MDSCs share phenotypic and functional similarities.

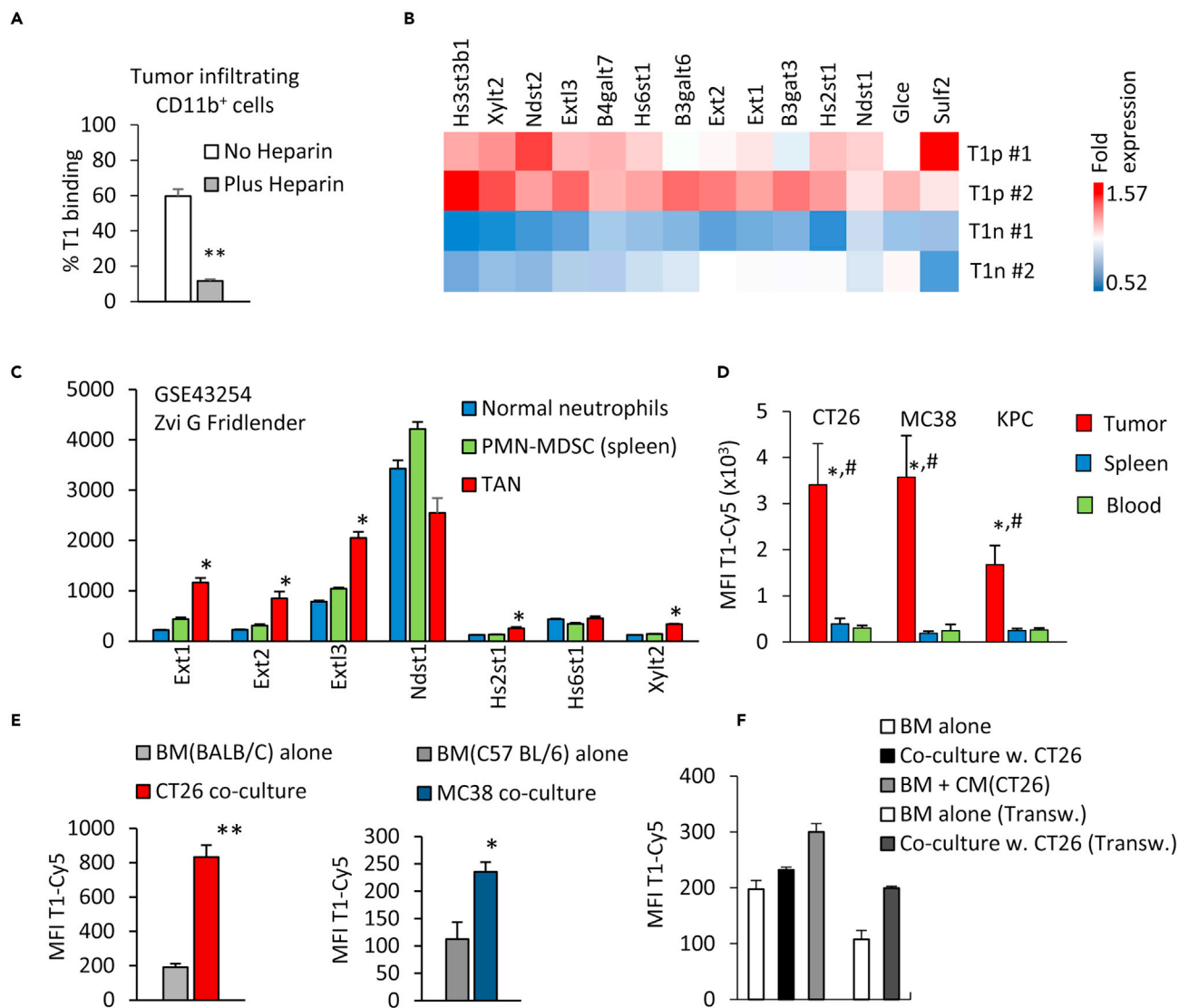


**Figure 6. Heparan sulfate biogenesis gene expression is increased in PMN-MDSCs upon entry into tumor leading to binding of T1 thioaptamer probe with higher affinity**

(A) CT26-tumor-associated leukocytes were isolated and analyzed for T1 binding in absence or presence of heparin (20ug/mL). Percentages of T1-Cy5 binding by CD45<sup>+</sup>/CD11b<sup>+</sup> population in absence or presence of heparin is shown represented as means with standard errors; n = 3 (three individual tumors analyzed); \*\*p < 0.01.

(B) Gene expression analysis of T1-binding Ly6G<sup>high</sup>T1p and T1 nonbinding Ly6G<sup>high</sup>T1n myeloid cell fractions isolated from CT26 tumor. Ly6G<sup>high</sup>T1p and Ly6G<sup>high</sup>T1n cells were subjected to gene set enrichment analysis (GSEA) with datasets related to heparan sulfate biosynthesis. Results were accepted at NOM p < 0.05, FDR q < 0.25. Heatmap shows heparan sulfate biogenesis genes with higher expression in Ly6G<sup>high</sup>T1p relative to Ly6G<sup>high</sup>T1n (including top ranked genes in GSEA).

(C) Gene expression dataset (GSE43254, deposited by Zvi G Fridlender) available at gene expression omnibus (NCBI) was analyzed for the expression of heparan sulfate biosynthesis genes in tumor-associated PMNs (TAN) relative to PMNs outside of tumor (normal neutrophils: neutrophils in tumor-free mice; PMN-MDSC (spleen): splenic PMNs of tumor-bearing mice). Data are represented as means with standard errors; \*p < 0.05 comparing TAN with normal neutrophils.

(D) Tumor, blood, and spleen of tumor-bearing mice (CT26, MC38, and KPC models) were analyzed for T1 binding by FACS. Results for T1 binding by CD45<sup>+</sup>CD11b<sup>+</sup>Ly6G<sup>high</sup> cell subset are shown and displayed as mean MFI of T1 binding with standard errors. \*p < 0.05 in student's t test comparing tumor and blood; #; p < 0.05 in student's t test comparing tumor and spleen. n = 3 per model.

(E) Naive mouse bone marrow (BM) cells were co-cultured with tumor cell lines CT26 and MC38, respectively, for 3 days. At end of culture period, T1 binding to CD11b<sup>+</sup>/Ly6G<sup>+</sup> cells was evaluated by measuring MFI of T1-Cy5 bound to the cells. Data are represented as means with standard errors. Representative results of two experiments are shown. Differences to BM-alone culture were evaluated by student's t test; \*p < 0.05, \*\*p < 0.01.

**Figure 6. Continued**

(F) BM and CT26 were co-cultured for 18 h. For comparison, BM was cultured with CT26-tumor-cell condition medium (CM), or BM and CT26 were separated by a membrane during co-culture in a transwell format (transw.). T1-binding was evaluated as in (E). See also [Figures S9–S11](#).

A number of approaches have been developed to indirectly inhibit tumor growth by targeting tumor-associated myeloid cells. However, a potential caveat is that they may not always discriminate between pro- and anti-tumor myeloid cell populations apparently present together in the tumor microenvironment ([Cassetta and Pollard, 2018](#); [Lavin et al., 2017](#); [Solito et al., 2014](#)). De La Fuente et al. recently reported RNA aptamers 3, 6, 11, and 14 isolated in a screen for targeting tumor-associated myeloid cells. Aptamers 3 and 11 bind to the receptors commonly expressed on myeloid cells, annexin A4 and vimentin, respectively. A mixture of the four aptamers was used to transport doxorubicin into tumors, which is likely to have bystander cell killing activity ([De La Fuente et al., 2020](#)). In our current study, T1 thioaptamer allowed an alternative therapeutic strategy by targeting the disease perpetuating MDSCs, without affecting tumor attacking mature subsets. Indeed, T1-guided delivery of chemotherapeutics oxaliplatin or doxorubicin showed improved effects in anti-tumor therapy. The cell specificity of T1 thioaptamer will also be an essential feature when combining with immunotherapy agents. In those scenarios, antigen-presenting myeloid cells will be needed for T cell activation, and we found that these myeloid subsets are less targeted by T1 thioaptamer.

In conclusion, we have found that tumor-associated MDSCs in colon and pancreatic cancer express heparan-sulfate-modified syndecan-1. Tumor microenvironment promotes high affinity binding between T1 and tumor-infiltrating MDSCs but not other cell types within tumors and in the periphery, an advantageous feature in therapeutic application limiting bystander cell damage. Thus, the T1 thioaptamer can serve as a useful tool for targeting MDSCs in tumor therapy. Furthermore, our findings support the concept that heparan-sulfate-modified syndecans control immature myeloid developmental status, a mechanism exploited by tumors to maintain immunosuppressive immature cells instead of host protective mature cells within their vicinity.

**Limitations of the study**

Our data strongly support a specifically modulated heparan sulfate on syndecan-1 as part of the binding site for a T1 thioaptamer probe. However, we do not know the exact molecular structure of this heparan sulfate chain. Based on current technology it is not feasible yet to determine the precise molecular composition of such complex sugar chains.

Regarding clinical application of T1 aptamer, liposomal oxaliplatin formulated with T1 showed greater efficacy in inhibiting tumor progression than free oxaliplatin in the preclinical colon cancer model CT26. However, we did not achieve tumor eradication. Therefore, despite this proof of principle result we need an optimization of the therapeutic T1 regimen to enhance its clinical value. First, driven by tumor-cell-derived factors PMN-MDSCs show a high regeneration rate, indicating that application of more than one single dose of drug may be warranted to deplete these cells for extended periods of time *in vivo*. Indeed, multiple treatments with T1 regimen had superior anti-tumor efficacy compared with single treatment. In recent preliminary studies, due to low systemic toxicity of T1-aptamer-guided liposomal chemotherapy-drug, it was feasible to give the drug every 3 days for 3 weeks without limiting toxic effects in mice. Second, the current study presents multiple evidences that T1 aptamer preferentially targets immunosuppressive myeloid cell types over nonsuppressive counterparts. Thus,

**Table 2. Heparan sulfate biogenesis genes are enriched in Ly6G<sup>high</sup>T1p cells<sup>a</sup>**

Gene set	NOM p-val	FDR q-val
KEGG glycosaminoglycan biosynthesis—heparan sulfate	0.00246	0.0173
Reactome heparan sulfate HS GAG metabolism	0.00677	0.0112
Reactome HS GAG degradation	0.0114	0.0108

<sup>a</sup>Transcriptomes of Ly6G<sup>high</sup>T1p and Ly6G<sup>high</sup>T1n cells were subjected to gene set enrichment analysis (GSEA) with datasets related to heparan sulfate biogenesis. Results were accepted at NOM p < 0.05, FDR q < 0.25.

it is an ideal candidate to reduce immunosuppression and support the action of immunotherapies such as adoptively transferred T cells, CAR T cells, tumor vaccines, etc. in a combination treatment approach.

## STAR★METHODS

Detailed methods are provided in the online version of this paper and include the following:

- KEY RESOURCES TABLE
- RESOURCE AVAILABILITY
  - Lead contact
  - Materials availability
  - Data and code availability
- EXPERIMENT MODEL AND SUBJECT DETAILS
  - Mouse models
  - Study cohorts
- METHODS DETAILS
  - Cell lines
  - Tissue/Blood preparation for T1 binding assay and flowcytometry
  - T1 binding assay
  - T1 binding assay with K562 leukemia cell line, heparin competition study
  - ROS assay
  - CYTOF
  - Bone marrow/tumor cell co-culture
  - Myeloid cell subset isolation by FACS
  - Transcriptomic analysis
  - T cell suppression assay, IFN $\gamma$  ELISpot
  - IFN $\gamma$  ELISpot
  - Mass spectrometric identification of T1 aptamer binding partner
  - CRISPR KO
  - Confocal microscopy
- QUANTIFICATION AND STATISTICAL ANALYSIS
  - Statistical analysis

## SUPPLEMENTAL INFORMATION

Supplemental information can be found online at <https://doi.org/10.1016/j.isci.2021.103349>.

## ACKNOWLEDGMENTS

We would like to thank Maricela Ramirez and Shuyue Zhou for excellent technical support and Louis Hinkle for text editing suggestions. The work was partially supported by National Institutes of Health grants U54CA210181, R01CA193880, and R01CA222959.

## AUTHOR CONTRIBUTIONS

Conception and design: H. Shen and T. Welte; Development of methodology: T. Welte, J. Mai, Z. Zhang, G. Zhang, and Y. Xu; Acquisition of data: T. Welte, S. Tian, and Y. Xu; Analysis and interpretation of data: T. Welte, H. Shen, T. Wang, J. Mai, Z. Zhang, L. Zhang, S. Tian, and S. Chen; Writing, review of manuscript: H. Shen, T. Welte, T. Wang, and S. Chen; Study supervision: H. Shen.

## DECLARATION OF INTERESTS

The authors declare no competing interests.

Received: June 24, 2021

Revised: September 17, 2021

Accepted: October 22, 2021

Published: November 19, 2021

**REFERENCES**

- Ahmadzadeh, M., Johnson, L.A., Heemskerck, B., Wunderlich, J.R., Dudley, M.E., White, D.E., and Rosenberg, S.A. (2009). Tumor antigen-specific CD8 T cells infiltrating the tumor express high levels of PD-1 and are functionally impaired. *Blood* 114, 1537–1544.
- Almand, B., Clark, J.I., Nikitina, E., van Beynen, J., English, N.R., Knight, S.C., Carbone, D.P., and Gabrilovich, D.I. (2001). Increased production of immature myeloid cells in cancer patients: a mechanism of immunosuppression in cancer. *J. Immunol.* 166, 678–689.
- Barber, D.L., Wherry, E.J., Masopust, D., Zhu, B., Allison, J.P., Sharpe, A.H., Freeman, G.J., and Ahmed, R. (2006). Restoring function in exhausted CD8 T cells during chronic viral infection. *Nature* 439, 682–687.
- Bernfield, M., Gotte, M., Park, P.W., Reizes, O., Fitzgerald, M.L., Lincecum, J., and Zako, M. (1999). Functions of cell surface heparan sulfate proteoglycans. *Annu. Rev. Biochem.* 68, 729–777.
- Bronte, V., Brandau, S., Chen, S.H., Colombo, M.P., Frey, A.B., Greten, T.F., Mandruzzato, S., Murray, P.J., Ochoa, A., Ostrand-Rosenberg, S., et al. (2016). Recommendations for myeloid-derived suppressor cell nomenclature and characterization standards. *Nat. Commun.* 7, 12150.
- Cassetta, L., and Pollard, J.W. (2018). Targeting macrophages: therapeutic approaches in cancer. *Nat. Rev. Drug Discov.* 17, 887–904.
- Chang, J.S., Santhanam, R., Trotta, R., Neviani, P., Eiring, A.M., Brierecheck, E., Ronchetti, M., Roy, D.C., Calabretta, B., Caligiuri, M.A., et al. (2007). High levels of the BCR/ABL oncoprotein are required for the MAPK-hnRNP-E2 dependent suppression of C/EBPalpha-driven myeloid differentiation. *Blood* 110, 994–1003.
- Chen, L., Diao, L., Yang, Y., Yi, X., Rodriguez, B.L., Li, Y., Villalobos, P.A., Cascone, T., Liu, X., Tan, L., et al. (2018). CD38-mediated immunosuppression as a mechanism of tumor cell escape from PD-1/PD-L1 blockade. *Cancer Discov.* 8, 1156–1175.
- Chopra, M., and Bohlander, S.K. (2019). The cell of origin and the leukemia stem cell in acute myeloid leukemia. *Genes Chromosomes Cancer* 58, 850–858.
- Christiansson, L., Soderlund, S., Svensson, E., Mustjoki, S., Bengtsson, M., Simonsson, B., Olsson-Stromberg, U., and Loskog, A.S. (2013). Increased level of myeloid-derived suppressor cells, programmed death receptor ligand 1/programmed death receptor 1, and soluble CD25 in Sokal high risk chronic myeloid leukemia. *PLoS One* 8, e55818.
- Chun, E., Lavoie, S., Michaud, M., Gallini, C.A., Kim, J., Soucy, G., Odze, R., Glickman, J.N., and Garrett, W.S. (2015). CCL2 promotes colorectal carcinogenesis by enhancing polymorphonuclear myeloid-derived suppressor cell population and function. *Cell Rep.* 12, 244–257.
- Day, C.L., Kaufmann, D.E., Kiepiela, P., Brown, J.A., Moodley, E.S., Reddy, S., Mackey, E.W., Miller, J.D., Leslie, A.J., DePierres, C., et al. (2006). PD-1 expression on HIV-specific T cells is associated with T-cell exhaustion and disease progression. *Nature* 443, 350–354.
- De Henau, O., Rausch, M., Winkler, D., Campesato, L.F., Liu, C., Cymerman, D.H., Budhu, S., Ghosh, A., Pink, M., Tchaicha, J., et al. (2016). Overcoming resistance to checkpoint blockade therapy by targeting PI3Kgamma in myeloid cells. *Nature* 539, 443–447.
- De La Fuente, A., Zilio, S., Caroli, J., Van Simaey, D., Mazza, E.M.C., Ince, T.A., Bronte, V., Biccato, S., Weed, D.T., and Serafini, P. (2020). Aptamers against mouse and human tumor-infiltrating myeloid cells as reagents for targeted chemotherapy. *Sci. Transl. Med.* 12, eaav9760.
- Dhanasekaran, R., Nakamura, I., Hu, C., Chen, G., Oseini, A.M., Seven, E.S., Miarni, A.G., Moser, C.D., Zhou, W., van Kuppevelt, T.H., et al. (2015). Activation of the transforming growth factor-beta/SMAD transcriptional pathway underlies a novel tumor-promoting role of sulfatase 1 in hepatocellular carcinoma. *Hepatology* 61, 1269–1283.
- Dziarski, R. (1989). Enhancement of mixed leukocyte reaction and cytotoxic antitumor responses by heparin. *J. Immunol.* 143, 356–365.
- El Ghazal, R., Yin, X., Johns, S.C., Swanson, L., Macal, M., Ghosh, P., Zuniga, E.I., and Fuster, M.M. (2016). Glycan sulfation modulates dendritic cell biology and tumor growth. *Neoplasia* 18, 294–306.
- Elinav, E., Nowarski, R., Thaiss, C.A., Hu, B., Jin, C., and Flavell, R.A. (2013). Inflammation-induced cancer: crosstalk between tumours, immune cells and microorganisms. *Nat. Rev. Cancer* 13, 759–771.
- Ellington, A.D., and Szostak, J.W. (1990). In vitro selection of RNA molecules that bind specific ligands. *Nature* 346, 818–822.
- Escobar Galvis, M.L., Jia, J., Zhang, X., Jastrebova, N., Spillmann, D., Gottfridsson, E., van Kuppevelt, T.H., Zcharia, E., Vlodyavsky, I., Lindahl, U., et al. (2007). Transgenic or tumor-induced expression of heparanase upregulates sulfation of heparan sulfate. *Nat. Chem. Biol.* 3, 773–778.
- Fan, H., Qiao, L., Kang, K.D., Fan, J., Wei, W., and Luo, G. (2017). Attachment and postattachment receptors important for hepatitis C virus infection and cell-to-cell transmission. *J. Virol.* 91, e00280-17.
- Fridlender, Z.G., Sun, J., Mishalian, I., Singhal, S., Cheng, G., Kapoor, V., Horng, W., Fridlender, G., Bayuh, R., Worthen, G.S., et al. (2012). Transcriptomic analysis comparing tumor-associated neutrophils with granulocytic myeloid-derived suppressor cells and normal neutrophils. *PLoS One* 7, e31524.
- Gabrilovich, D.I., Ostrand-Rosenberg, S., and Bronte, V. (2012). Coordinated regulation of myeloid cells by tumours. *Nat. Rev. Immunol.* 12, 253–268.
- Giallongo, C., Parrinello, N., Tibullo, D., La Cava, P., Romano, A., Chiarenza, A., Barbagallo, I., Palumbo, G.A., Stagno, F., Vigneri, P., et al. (2014). Myeloid derived suppressor cells (MDSCs) are increased and exert immunosuppressive activity together with polymorphonuclear leukocytes (PMNs) in chronic myeloid leukemia patients. *PLoS One* 9, e101848.
- Gonda, K., Shibata, M., Ohtake, T., Matsumoto, Y., Tachibana, K., Abe, N., Ohto, H., Sakurai, K., and Takenoshita, S. (2017). Myeloid-derived suppressor cells are increased and correlated with type 2 immune responses, malnutrition, inflammation, and poor prognosis in patients with breast cancer. *Oncol. Lett.* 14, 1766–1774.
- Heine, A., Held, S.A.E., Schulte-Schrepping, J., Wolff, J.F.A., Klee, K., Ulas, T., Schmacke, N.A., Daecke, S.N., Riethausen, K., Schultze, J.L., et al. (2017). Generation and functional characterization of MDSC-like cells. *Oncoimmunology* 6, e1295203.
- Herber, D.L., Cao, W., Nefedova, Y., Novitskiy, S.V., Nagaraj, S., Tyurin, V.A., Corzo, A., Cho, H.I., Celis, E., Lennox, B., et al. (2010). Lipid accumulation and dendritic cell dysfunction in cancer. *Nat. Med.* 16, 880–886.
- Highfill, S.L., Cui, Y., Giles, A.J., Smith, J.P., Zhang, H., Morse, E., Kaplan, R.N., and Mackall, C.L. (2014). Disruption of CXCR2-mediated MDSC tumor trafficking enhances anti-PD1 efficacy. *Sci. Transl. Med.* 6, 237ra267.
- Holtzhausen, A., Harris, W., Ubil, E., Hunter, D.M., Zhao, J., Zhang, Y., Zhang, D., Liu, Q., Wang, X., Graham, D.K., et al. (2019). TAM family receptor kinase inhibition reverses MDSC-mediated suppression and augments anti-PD-1 therapy in melanoma. *Cancer Immunol. Res.* 7, 1672–1686.
- Hossain, M.M., Hosono-Fukao, T., Tang, R., Sugaya, N., van Kuppevelt, T.H., Jenniskens, G.J., Kimata, K., Rosen, S.D., and Uchimura, K. (2010). Direct detection of HSulf-1 and HSulf-2 activities on extracellular heparan sulfate and their inhibition by PI-88. *Glycobiology* 20, 175–186.
- Khurana, A., Tun, H.W., Marlow, L., Copland, J.A., Dredge, K., and Shridhar, V. (2012). Hypoxia negatively regulates heparan sulfatase 2 expression in renal cancer cell lines. *Mol. Carcinog.* 51, 565–575.
- Kiefer, M.C., Ishihara, M., Swiedler, S.J., Crawford, K., Stephens, J.C., and Barr, P.J. (1991). The molecular biology of heparan sulfate fibroblast growth factor receptors. *Ann. N. Y. Acad. Sci.* 638, 167–176.
- Kim, K., Skora, A.D., Li, Z., Liu, Q., Tam, A.J., Blosser, R.L., Diaz, L.A., Jr., Papadopoulos, N., Kinzler, K.W., Vogelstein, B., et al. (2014). Eradication of metastatic mouse cancers resistant to immune checkpoint blockade by suppression of myeloid-derived cells. *Proc. Natl. Acad. Sci. U S A.* 111, 11774–11779.
- Kudo-Saito, C., Shirako, H., Ohike, M., Tsukamoto, N., and Kawakami, Y. (2013). CCL2 is critical for immunosuppression to promote cancer metastasis. *Clin. Exp. Metastasis* 30, 393–405.
- Kurup, S., Wijnhoven, T.J., Jenniskens, G.J., Kimata, K., Habuchi, H., Li, J.P., Lindahl, U., van Kuppevelt, T.H., and Spillmann, D. (2007). Characterization of anti-heparan sulfate phage

display antibodies AO4B08 and HS4E4. *J. Biol. Chem.* **282**, 21032–21042.

Kwack, K.H., and Lee, H.W. (2017). Progranulin inhibits human T lymphocyte proliferation by inducing the formation of regulatory T lymphocytes. *Mediat. Inflamm.* **2017**, 7682083.

Lavin, Y., Kobayashi, S., Leader, A., Amir, E.D., Elefant, N., Bigenwald, C., Remark, R., Sweeney, R., Becker, C.D., Levine, J.H., et al. (2017). Innate immune landscape in early lung adenocarcinoma by paired single-cell analyses. *Cell* **169**, 750–765 e17.

Lee-Sherick, A.B., Jacobsen, K.M., Henry, C.J., Huey, M.G., Parker, R.E., Page, L.S., Hill, A.A., Wang, X., Frye, S.V., Earp, H.S., et al. (2018). MERTK inhibition alters the PD-1 axis and promotes anti-leukemia immunity. *JCI Insight* **3**, e97941.

Li, J., Shworak, N.W., and Simons, M. (2002a). Increased responsiveness of hypoxic endothelial cells to FGF2 is mediated by HIF-1 $\alpha$ -dependent regulation of enzymes involved in synthesis of heparan sulfate FGF2-binding sites. *J. Cell Sci.* **115**, 1951–1959.

Li, Q., Park, P.W., Wilson, C.L., and Parks, W.C. (2002b). Matrilysin shedding of syndecan-1 regulates chemokine mobilization and transepithelial efflux of neutrophils in acute lung injury. *Cell* **111**, 635–646.

Liu, H., Mai, J., Shen, J., Wolfram, J., Li, Z., Zhang, G., Xu, R., Li, Y., Mu, C., Zu, Y., et al. (2018). A novel DNA aptamer for dual targeting of polymorphonuclear myeloid-derived suppressor cells and tumor cells. *Theranostics* **8**, 31–44.

Ma, Y., Li, X., Li, W., and Liu, Z. (2018). Glycan-imprinted magnetic nanoparticle-based SELEX for efficient screening of glycoprotein-binding aptamers. *ACS Appl. Mater. Inter.* **10**, 40918–40926.

Mai, J., Li, X., Zhang, G., Huang, Y., Xu, R., Shen, Q., Lokesh, G.L., Thiviyathan, V., Chen, L., Liu, H., et al. (2018). DNA thioaptamer with homing specificity to lymphoma bone marrow involvement. *Mol. Pharm.* **15**, 1814–1825.

Marigo, I., Trovato, R., Hofer, F., Ingangi, V., De Sanctis, F., Ugel, S., Cane, S., Simonelli, A., Lamolinara, A., Iezzi, M., et al. (2020). The Disabled homolog 2 controls pro-metastatic activity of tumor-associated macrophages. *Cancer Discov.* **10**:1758–1773.

Mastio, J., Condamine, T., Dominguez, G., Kossenkov, A.V., Donthireddy, L., Veglia, F., Lin, C., Wang, F., Fu, S., Zhou, J., et al. (2019). Identification of monocyte-like precursors of granulocytes in cancer as a mechanism for accumulation of PMN-MDSCs. *J. Exp. Med.* **216**, 2150–2169.

McRae, E.K.S., Booy, E.P., Padilla-Meier, G.P., and McKenna, S.A. (2017). On characterizing the interactions between proteins and guanine quadruplex structures of nucleic acids. *J. Nucleic Acids* **2017**, 9675348.

Mi, J., Liu, Y., Rabbani, Z.N., Yang, Z., Urban, J.H., Sullenger, B.A., and Clary, B.M. (2010). In vivo selection of tumor-targeting RNA motifs. *Nat. Chem. Biol.* **6**, 22–24.

Molgora, M., Esaulova, E., Vermi, W., Hou, J., Chen, Y., Luo, J., Brioschi, S., Bugatti, M., Omodei, A.S., Ricci, B., et al. (2020). TREM2 modulation remodels the tumor myeloid landscape enhancing anti-PD-1 immunotherapy. *Cell* **182**, 886–900 e17.

Nagaraj, S., Schrum, A.G., Cho, H.I., Celis, E., and Gabrilovich, D.I. (2010). Mechanism of T cell tolerance induced by myeloid-derived suppressor cells. *J. Immunol.* **184**, 3106–3116.

Ostrand-Rosenberg, S., and Fenselau, C. (2018). Myeloid-derived suppressor cells: immune-suppressive cells that impair antitumor immunity and are sculpted by their environment. *J. Immunol.* **200**, 422–431.

Pasqualon, T., Lue, H., Groening, S., Pruessmeyer, J., Jahr, H., Denecke, B., Bernhagen, J., and Ludwig, A. (2016). Cell surface syndecan-1 contributes to binding and function of macrophage migration inhibitory factor (MIF) on epithelial tumor cells. *Biochim. Biophys. Acta* **1863**, 717–726.

Peng, D.H., Rodriguez, B.L., Diao, L., Chen, L., Wang, J., Byers, L.A., Wei, Y., Chapman, H.A., Yamauchi, M., Behrens, C., et al. (2020). Collagen promotes anti-PD-1/PD-L1 resistance in cancer through LAIR1-dependent CD8(+) T cell exhaustion. *Nat. Commun.* **11**, 4520.

Pinhal, M.A., Smith, B., Olson, S., Aikawa, J., Kimata, K., and Esko, J.D. (2001). Enzyme interactions in heparan sulfate biosynthesis: uronosyl 5-epimerase and 2-O-sulfotransferase interact in vivo. *Proc. Natl. Acad. Sci. U S A.* **98**, 12984–12989.

Pzyer, A.R., Stroopinsky, D., Rajabi, H., Washington, A., Tagde, A., Coll, M., Fung, J., Bryant, M.P., Cole, L., Palmer, K., et al. (2017). MUC1-mediated induction of myeloid-derived suppressor cells in patients with acute myeloid leukemia. *Blood* **129**, 1791–1801.

Reiland, J., Sanderson, R.D., Waguespack, M., Barker, S.A., Long, R., Carson, D.D., and Marchetti, D. (2004). Heparanase degrades syndecan-1 and perlecan heparan sulfate: functional implications for tumor cell invasion. *J. Biol. Chem.* **279**, 8047–8055.

Ren, Z., van Andel, H., de Lau, W., Hartholt, R.B., Maurice, M.M., Clevers, H., Kersten, M.J., Spaargaren, M., and Pals, S.T. (2018). Syndecan-1 promotes Wnt/ $\beta$ -catenin signaling in multiple myeloma by presenting Wnts and R-spondins. *Blood* **131**, 982–994.

Rosenbauer, F., and Tenen, D.G. (2007). Transcription factors in myeloid development: balancing differentiation with transformation. *Nat. Rev. Immunol.* **7**, 105–117.

Roumenina, L.T., Daugan, M.V., Noe, R., Petitprez, F., Vano, Y.A., Sanchez-Salas, R., Becht, E., Meilleroux, J., Clec'h, B.L., Giraldo, N.A., et al. (2019a). Tumor cells hijack macrophage-produced complement C1q to promote tumor growth. *Cancer Immunol. Res.* **7**, 1091–1105.

Roumenina, L.T., Daugan, M.V., Petitprez, F., Sautes-Fridman, C., and Fridman, W.H. (2019b). Context-dependent roles of complement in cancer. *Nat. Rev. Cancer* **19**, 698–715.

Saleh, M.E., Gadalla, R., Hassan, H., Afifi, A., Gotte, M., El-Shinawi, M., Mohamed, M.M., and Ibrahim, S.A. (2019). The immunomodulatory role of tumor Syndecan-1 (CD138) on ex vivo tumor microenvironmental CD4+ T cell polarization in inflammatory and non-inflammatory breast cancer patients. *PLoS One* **14**, e0217550.

Shen, L., Li, H., Shi, Y., Wang, D., Gong, J., Xun, J., Zhou, S., Xiang, R., and Tan, X. (2016). M2 tumour-associated macrophages contribute to tumour progression via legumain remodelling the extracellular matrix in diffuse large B cell lymphoma. *Sci. Rep.* **6**, 30347.

Simpson, K.D., Templeton, D.J., and Cross, J.V. (2012). Macrophage migration inhibitory factor promotes tumor growth and metastasis by inducing myeloid-derived suppressor cells in the tumor microenvironment. *J. Immunol.* **189**, 5533–5540.

Sinha, P., Parker, K.H., Horn, L., and Ostrand-Rosenberg, S. (2012). Tumor-induced myeloid-derived suppressor cell function is independent of IFN- $\gamma$  and IL-4R $\alpha$ . *Eur. J. Immunol.* **42**, 2052–2059.

Solito, S., Marigo, I., Pinton, L., Damuzzo, V., Mandruzzato, S., and Bronte, V. (2014). Myeloid-derived suppressor cell heterogeneity in human cancers. *Ann. N. Y. Acad. Sci.* **1319**, 47–65.

Suhovskih, A.V., Tsidulko, A.Y., Kutsenko, O.S., Kovner, A.V., Aidagulova, S.V., Ernberg, I., and Grigorieva, E.V. (2014). Transcriptional activity of heparan sulfate biosynthetic machinery is specifically impaired in benign prostate hyperplasia and prostate cancer. *Front. Oncol.* **4**, 79.

Swart, M., and Troeberg, L. (2019). Effect of polarization and chronic inflammation on macrophage expression of heparan sulfate proteoglycans and biosynthesis enzymes. *J. Histochem. Cytochem.* **67**, 9–27.

Tcyganov, E., Mastio, J., Chen, E., and Gabrilovich, D.I. (2018). Plasticity of myeloid-derived suppressor cells in cancer. *Curr. Opin. Immunol.* **51**, 76–82.

Terstappen, L.W., Safford, M., Unterhalt, M., Konemann, S., Zurlutter, K., Piechotka, K., Drescher, M., Aul, C., Buchner, T., Hiddemann, W., et al. (1992). Flow cytometric characterization of acute myeloid leukemia: IV. Comparison to the differentiation pathway of normal hematopoietic progenitor cells. *Leukemia* **6**, 993–1000.

Tuerk, C., and Gold, L. (1990). Systematic evolution of ligands by exponential enrichment: RNA ligands to bacteriophage T4 DNA polymerase. *Science* **249**, 505–510.

van den Born, J., Salmivirta, K., Henttinen, T., Ostman, N., Ishimaru, T., Miyaura, S., Yoshida, K., and Salmivirta, M. (2005). Novel heparan sulfate structures revealed by monoclonal antibodies. *J. Biol. Chem.* **280**, 20516–20523.

van Gemst, J.J., Kouwenberg, M., Rops, A., van Kuppevelt, T.H., Berden, J.H., Rabelink, T.J., Loeven, M.A., and van der Vlag, J. (2018). Differential binding of chemokines CXCL1, CXCL2 and CCL2 to mouse glomerular endothelial cells reveals specificity for distinct heparan sulfate domains. *PLoS One* **13**, e0201560.

Veglia, F., Hashimoto, A., Dweep, H., Sanseviero, E., De Leo, A., Tcyganov, E., Kossenkov, A., Mulligan, C., Nam, B., Masters, G., et al. (2021). Analysis of classical neutrophils and polymorphonuclear myeloid-derived suppressor cells in cancer patients and tumor-bearing mice. *J. Exp. Med.* *218*, e20201803.

Vinkenburg, J.L., Mayer, G., and Famulok, M. (2012). Aptamer-based affinity labeling of proteins. *Angew. Chem. Int. Ed. Engl.* *51*, 9176–9180.

Wang, T., Yu, H., Hughes, N.W., Liu, B., Kendirli, A., Klein, K., Chen, W.W., Lander, E.S., and Sabatini, D.M. (2017). Gene essentiality profiling reveals gene networks and synthetic lethal interactions with oncogenic Ras. *Cell* *168*, 890–903 e15.

Weide, B., Martens, A., Zelba, H., Stutz, C., Derhovanessian, E., Di Giacomo, A.M., Maio, M., Sucker, A., Schilling, B., Schadendorf, D., et al. (2014). Myeloid-derived suppressor cells predict survival of patients with advanced melanoma:

comparison with regulatory T cells and NY-ESO-1- or melan-A-specific T cells. *Clin. Cancer Res.* *20*, 1601–1609.

Welte, T., Kim, I.S., Tian, L., Gao, X., Wang, H., Li, J., Holdman, X.B., Herschkowitz, J.I., Pond, A., Xie, G., et al. (2016). Oncogenic mTOR signalling recruits myeloid-derived suppressor cells to promote tumour initiation. *Nat. Cell Biol.* *18*, 632–644.

Won, H., Moreira, D., Gao, C., Dutttagupta, P., Zhao, X., Manuel, E., Diamond, D., Yuan, Y.C., Liu, Z., Jones, J., et al. (2017). TLR9 expression and secretion of LIF by prostate cancer cells stimulates accumulation and activity of polymorphonuclear MDSCs. *J. Leukoc. Biol.* *102*, 423–436.

Yang, M., Liu, J., Shao, J., Qin, Y., Ji, Q., Zhang, X., and Du, J. (2014). Cathepsin S-mediated autophagic flux in tumor-associated macrophages accelerate tumor development

by promoting M2 polarization. *Mol. Cancer* *13*, 43.

Zhang, Y., Wang, N., Raab, R.W., McKown, R.L., Irwin, J.A., Kwon, I., van Kuppevelt, T.H., and Laurie, G.W. (2013). Targeting of heparanase-modified syndecan-1 by prosecretory mitogen lacritin requires conserved core GAGAL plus heparan and chondroitin sulfate as a novel hybrid binding site that enhances selectivity. *J. Biol. Chem.* *288*, 12090–12101.

Zhou, J., and Rossi, J. (2017). Aptamers as targeted therapeutics: current potential and challenges. *Nat. Rev. Drug Discov.* *16*, 440.

Zhou, G., Sprengers, D., Boor, P.P.C., Doukas, M., Schutz, H., Mancham, S., Pedroza-Gonzalez, A., Polak, W.G., de Jonge, J., Gaspersz, M., et al. (2017). Antibodies against immune checkpoint molecules restore functions of tumor-infiltrating T cells in hepatocellular carcinomas. *Gastroenterology* *153*, 1107–1119 e10.

STAR★METHODS

KEY RESOURCES TABLE

REAGENT or RESOURCE	SOURCE	IDENTIFIER
<b>Antibodies</b>		
$\alpha$ biotin	Biologend (San Diego, CA)	Clone 1D4-C5
$\alpha$ mouse CD45.2	Tonbo (San Diego, CA)	Clone 104
$\alpha$ mouse CD45	Tonbo (San Diego, CA)	Clone 30-F11
FcR shield ( $\alpha$ mou CD16/32)	Biologend (San Diego, CA)	Cat.nr. 101302
$\alpha$ mouse Ly6G-FITC	Biologend (San Diego, CA)	Clone 1A8
$\alpha$ mouse Ly6C-PECy7	Biologend (San Diego, CA)	Clone HK1.4
$\alpha$ hu/mou CD11b-APC Cy7	Tonbo (San Diego, CA)	Clone M1/70
$\alpha$ mouse syndecan-1 PE	Biologend (San Diego, CA)	Clone 281-2
$\alpha$ human syndecan-1-PE	Biologend (San Diego, CA)	Clone DL101
$\alpha$ mouse syndecan-3	R&D Systems (Minneapolis, MN)	Clone AF2734
$\alpha$ heparin/heparan sulfate	MilliporeSigma (St. Louis, MO)	MAB2040
$\alpha$ mouse IgG-AF488	Thermo Fisher Sc. (Waltham, MA)	Cat.nr. A11001
$\alpha$ goat IgG-AF350	Thermo Fisher Sc. (Waltham, MA)	Cat.nr. A21081
$\alpha$ mouse CD3e	Tonbo (San Diego, CA)	Clone 145-2C11
$\alpha$ mouse CD4	Biologend (San Diego, CA)	Clone GK1.4
$\alpha$ mouse CD8a	Tonbo (San Diego, CA)	Clone 53-6.7
$\alpha$ mouse PD-1	Biologend (San Diego, CA)	Clone RMP1-14
$\alpha$ mouse PD-L1	BD Biosciences (San Jose, CA)	Clone MIH5
Streptavidin-PE	Tonbo (San Diego, CA, USA)	Cat.nr.50-4317-u100
CFSE	Thermo Fisher Sc. (Waltham, MA)	Cell Trace CFSE
<b>Chemicals, peptides, and recombinant proteins</b>		
Ova-1 peptide	Peptide 2.0 (Chantilly, VA)	Sequence: SIINFEKL
Ova-2 peptide	Peptide 2.0 (Chantilly, VA)	Sequence: ISQAVHAHAHAEINEAGR
Collagenase type IV	Worthington (Lakewood, NJ)	Cat.nr. LS004188
DNase I	Worthington (Lakewood, NJ)	Cat.nr. LS006344
ACK red blood cell lysis	K D Medical (Columbia, MD)	Cat.nr. RGF-3015
mouse bFGF	Peprotech (Cranbury, NJ)	Cat.nr. 450-33
mouse EGF	Peprotech (Cranbury, NJ)	Cat.nr. 315-09
mouse IL-2	Peprotech (Cranbury, NJ)	Cat.nr. 212-12-5ug
B27	Thermo Fisher Sc. (Waltham, MA)	Cat.nr. 17504044
Heparin	MilliporeSigma (St. Louis, MO)	Cat.nr. H3149-250ku
Chondroitin sulfate	MilliporeSigma (St. Louis, MO)	Cat.nr. C9819-5G
Hyaluronic acid	MilliporeSigma (St. Louis, MO)	Cat.nr. H6388-100mg
pLE400 (MW 60,000 Da)	Alamanda Polym. (Huntsville, AL)	CAS nr. 26247-79-0
human heparanase I	Thermo Fisher Sc. (Waltham, MA)	Cat.nr. 7570GH005
Heparinase I-III	MilliporeSigma (St. Louis, MO)	Cat.nr. H3917-50un
Oxaliplatin	Selleck Biochem (Houston, TX)	Cat.nr. S1224
DSPE-PEG-Mal	Avanti Polar Lipids (Alabaster, AL)	Full name in <a href="#">Liu et al., 2018</a>
DPPC	Avanti Polar Lipids (Alabaster, AL)	Full name in <a href="#">Liu et al., 2018</a>
Cholesterol	MilliporeSigma (St. Louis, MO)	Cat.nr. C8667-25G
DSPE-PEG(2000)	Avanti Polar Lipids (Alabaster, AL)	Full name in <a href="#">Liu et al., 2018</a>

(Continued on next page)

<b>Continued</b>		
REAGENT or RESOURCE	SOURCE	IDENTIFIER
<b>Critical commercial assays</b>		
Counting beads	Thermo Fisher Sc. (Waltham, MA)	Cat.nr. C36950
CellROX ROS Deep Red	Thermo Fisher Sc. (Waltham, MA)	Cat.nr. C10422
RNeasy Plus Micro Kit	Qiagen (Germantown, MD)	Cat.nr. 74034
mouse IFN $\gamma$ ELISpot	BD Biosciences (San Jose, CA)	Cat.nr. 551881
T cell isolation kit	StemCell Tech Vancouver, Canada	Cat.nr. 19851A
Thy1.2 T cell isolation kit	StemCell Tech Vancouver, Canada	Cat.nr. 18951
<b>Deposited data</b>		
RNA sequ. Raw data	This paper	GEO: GSE185974
<b>Experimental models: Cell lines</b>		
CT26	ATCC (Manassas, VA)	CRL-2638
K562	ATCC (Manassas, VA)	CCL-243
<b>Experimental models: Organisms/strains</b>		
BALB/C	Charles River (Wilmington, MA)	Strain code 028
C57BL/6	Charles River (Wilmington, MA)	Strain code 027
OT1	The Jackson Lab (Bar Harbor, ME)	Stock nr. 003831
DO11.10	The Jackson Lab (Bar Harbor, ME)	Stock nr. 003303
<b>Oligonucleotides</b>		
T1 aptamer	IdT Technologies (Coralville, IA)	Sequence in <a href="#">Liu et al., 2018</a>
Cy5-T1 aptamer	IdT Technologies (Coralville, IA)	Sequence in <a href="#">Liu et al., 2018</a>
5' SH-T1 aptamer	IdT Technologies (Coralville, IA)	Sequence in <a href="#">Liu et al., 2018</a>
ABAL	MilliporeSigma (St. Louis, MO)	Structure in <a href="#">Vinkenburg et al., 2012</a>
ABAL-T1 aptamer	IdT Technologies (Coralville, IA)	Sequence in <a href="#">Liu et al., 2018</a>
Cy5-SCR aptamer	IdT Technologies (Coralville, IA)	Sequence in <a href="#">Liu et al., 2018</a>
Cy5-ESTA aptamer	IdT Technologies (Coralville, IA)	Sequence in <a href="#">Mai et al., 2018</a>
<b>Recombinant DNA</b>		
pLenti-CAS9-GFP	Addgene (Watertown, MA)	Addgene #86145 in <a href="#">Wang et al., 2017</a>
pLentiGuide-gRNA(SDC-1)	Genscript Biotech (Piscataway, NJ)	gRNA sequence in <a href="#">Fan et al., 2017</a>
pLentiGuide-gRNA(EXT-1)	Genscript Biotech (Piscataway, NJ)	gRNA sequence in <a href="#">Ren et al., 2018</a>
<b>Software and algorithms</b>		
Image J	NIH	<a href="https://imagej.nih.gov/ij/">https://imagej.nih.gov/ij/</a> RRID:SCR_003070
GraphPad prism	GraphPad Software	<a href="https://www.graphpad.com/">https://www.graphpad.com/</a> RRID: SCR_002798
FlowJo	FlowJo	<a href="https://www.flowjo.com/">https://www.flowjo.com/</a> RRID: SCR_008520
GSEA	UC San Diego/Broad Institute	<a href="https://www.gsea-msigdb.org/gsea/">https://www.gsea-msigdb.org/gsea/</a> RRID: SCR_003199

## RESOURCE AVAILABILITY

### Lead contact

Further information and requests for resources and reagents should be directed to and will be fulfilled by the lead contact, Haifa Shen ([Hshen@houstonmethodist.org](mailto:Hshen@houstonmethodist.org)).

### Materials availability

CRISPR KO lines of K562 cells that were generated in this study (SDC-1 KO and EXT-1 KO) and parental K562 expressing GFP-CAS9 will be available upon reasonable request.

### Data and code availability

Data reported in this paper will be shared by the lead contact upon request. RNA sequ data were deposited in NCBI's Gene Expression Omnibus; Accession number GSE185974. This paper does not report original code. Any additional information required to reanalyze the data reported in this paper is available from the lead contact upon request.

## EXPERIMENT MODEL AND SUBJECT DETAILS

### Mouse models

All procedures on animals were performed following protocols approved by the Institutional Animal Care and Use Committee (IACUC) at Houston Methodist Research Institute. Tumor implantation studies were done with BALB/C and C57 BL/6 mice purchased from Charles River Laboratories (Boston, MA, USA) at 6 to 10 weeks of age. Both sexes were used equally for colon cancer (CT26, MC38) and pancreatic cancer (KPC) mouse models. CT26, MC38 and KPC tumor cells were injected subcutaneously in the flank of the animal at  $0.5 \times 10^6$  cells in 67  $\mu$ l PBS + 33  $\mu$ l matrigel per mouse utilizing mice of matching genetic background (BALB/C for CT26, C57BL/6 for MC38 and KPC, respectively). For orthotopic injections, approved, appropriate analgetic and anesthesia regimen were applied. CT26 and MC38 cells were injected to the cecum wall. KPC cells were injected to the pancreas. Tumor cell numbers were the same as for subcutaneous injection. After surgery, recovery of animals was frequently monitored.

OT1 mice serving as the resource for OVA-1 peptide specific T cells on C57BL/6 background, and DO11.10 mice transgenic for OVA-2 peptide specific TCR on BALB/C background were purchased from The Jackson Laboratory.

### Study cohorts

In tumor-therapy experiments, CT26 tumor-bearing BALB/C mice (age 6-12 weeks) were divided into experimental groups such that each group contained the same number of mice, and mean tumor size at the beginning of the experiment was similar in each group. Mice were treated twice with non-liposomal oxaliplatin, or oxaliplatin in T1 aptamer-tagged liposomes, or in random-sequence (SCR) aptamer-tagged liposomes, as indicated in figures, with treatment 1 on day 0 of measurements, and treatment 2 on day 7. Therapeutic drugs were injected intravenously at the indicated amounts in a 100  $\mu$ l volume. Control groups received aqueous vehicle only. Tumor size was determined by measuring length and width of tumor mass with a caliper and calculating tumor volume with the formula  $V=L*W^2*3.14/6$ .

## METHODS DETAILS

### Cell lines

Mouse colon cancer cell line CT26 and human chronic myelogenous leukemia cell line K562 were purchased from ATCC (Manassas, VA). Mouse pancreatic cancer cell line KPC was a kind gift of Dr. Sankar Mitra's group at Houston Methodist. Tumor cell lines were cultured in DMEM with high glucose, 10% FBS, and anti-biotic/anti-mitotic reagent. K562 cells were cultured in RPMI-1640, 10% FBS, and anti-biotic/anti-mitotic reagent.

### Tissue/Blood preparation for T1 binding assay and flowcytometry

Mouse tumors were excised, necrotic areas were discarded. Tumors were dissociated with collagenase type IV (0.8 mg/ml, Worthington, Lakewood, NJ) in presence of DNase I (50 u/ml, MilliporeSigma, St. Louis, MO), followed by gentle homogenization through cell strainer. Spleen tissue was disrupted by homogenization through cell strainer. Blood samples of mice were collected in EDTA coated tubes. Samples were centrifuged at 500 g for 5 min. All tissue-samples were submitted to ACK red blood cell lysis and wash steps at end of isolation procedure.

### T1 binding assay

Cell suspensions were incubated 30 min on ice with Cy5-labeled T1 aptamer (T1-Cy5, sequence shown in [Liu et al., 2018](#)), IDT Technologies, Coralville, Iowa). Binding buffer contained PBS, 2% FBS, 0.45 mg/ml D-glucose, 5 mM MgCl<sub>2</sub>, 125  $\mu$ g/ml yeast tRNA and 10  $\mu$ g/ml salmon sperm DNA. When additional antibody staining was performed, FcR shield was added at 0.5  $\mu$ g per  $1 \times 10^6$  cells. Fluorescently labeled antibodies to identify cell lineages were applied in parallel with T1-Cy5. DAPI was used for dead cell exclusion

and counting beads (Count bright absolute counting beads, Thermo Fisher Scientific, Waltham, MA) were added for cell number quantification. Non-fixed samples were immediately submitted to flow cytometry on LSR II or Fortessa instruments (BD Biosciences, San Jose, CA). Data analysis including tSNE was done using FlowJo\_V10\_CL software.

### T1 binding assay with K562 leukemia cell line, heparin competition study

T1 binding conditions were identical as with tumor-associated myeloid cells. In competition studies, cells were pre-treated with indicated amounts of competitor for 15 min on ice prior to the addition of T1-Cy5. Heparin from porcine intestinal mucosa was purchased from MilliporeSigma, St. Louis, MO. pLE400 was from Alamanda Polymers (Huntsville, AL). As a specificity control, T1 aptamer binding was compared to an E-selectin-specific aptamer (ESTA, (Mai et al., 2018)). In heparinase treatment studies, cells were pre-treated with the enzyme for 60 minutes at 37°, followed by three washes and T1 binding assay (Reiland et al., 2004). Bacterial heparinases I and III were applied at 0.4 units per 100,000 cells in a buffer containing 1 mM CaCl<sub>2</sub>, 1 mM HEPES, pH8 and 1% FBS in PBS.

### ROS assay

Cell suspensions were treated with CellROX Deep Red reagent (Thermo Fisher Scientific, Waltham, MA) at 5 μM for 30 min at 37°C, washed and submitted to T1 binding assay and FACS. Instead of T1-Cy5, biotinylated T1 was used in binding assays, followed by Streptavidin-PE detection, as CellROX was detected in same channel as Cy5.

### CYTOF

To detect T1-binding cells in CYTOF, a biotinylated T1 aptamer was used. Anti-biotin antibody (clone 1D4-C5, Biolegend) was labeled with a metal suitable for CYTOF detection using metal-labeling kit (Maxpar X8 Multimetal Labeling Kit, Fluidigm, South San Francisco, CA). The CD45<sup>+</sup> fraction of CT26 tumors was first incubated with T1-biotin. Next, sample was stained with metal-labeled anti-biotin in parallel with antibodies against 30 cell-type markers. After T1-binding and antibody staining, samples were further processed according to a standard CYTOF protocol at HMRI-ImmunoMonitoring Core, Houston Methodist Academic Institute). Two different antibodies against CD45 were used during cell enrichment and CYTOF detection stages to avoid binding interference (anti-CD45.2 clone 104 and anti-CD45 clone 30-F11, TONBO, San Diego, CA).

### Bone marrow/tumor cell co-culture

Mouse bone marrow (BM) was isolated from tibia and femur by flushing out cells in PBS with 10-ml syringe fitted with a 27<sup>1</sup>/<sub>2</sub> G needle, followed by elutriation. Bone marrow and tumor cells were co-cultured as described (Welte et al., 2016). Briefly, bone marrow cells were flushed from tibia and femur of naïve mice, treated with RBC lysis buffer, washed and cultured in absence or presence of tumor cells (ratio BM:tumor cells = 5:1) in a tumor sphere formation medium without FBS, with B27 supplement, bFGF (20 ng/ml) and EGF (20 ng/ml) in low adhesion plates. In mechanistic studies, cell types were separated in the chambers of a trans-well culture plate as indicated, with a 3 μm-pore size membrane between the chambers. Conditioned medium (CM) from CT26 tumor-cells cultured alone in tumor sphere medium for 24 h was cleared from cells and cell debris by centrifugation and used to treat BM cells in another experimental group. At end of culture period cells were analyzed by T1-Cy5 binding assay and antibody staining. In FACS analysis of bone marrow:tumor cell co-cultures, bone marrow-derived cells were discriminated from tumor cells based on SSC-A and FSC-A properties, and positive staining for CD45. Live (DAPI-negative) lineage-marker positive cells were enumerated utilizing counting beads.

### Myeloid cell subset isolation by FACS

Tumor cell suspensions were submitted to T1-Cy5 binding assay and staining with antibodies for cell-lineage identification. The following three subsets were sorted: (1) Ly6G<sup>high</sup>T1p = DAPI<sup>-</sup>CD45<sup>+</sup>CD11b<sup>+</sup>Ly6G<sup>++</sup>T1-Cy5<sup>+</sup>, (2) Ly6G<sup>high</sup>T1n = DAPI<sup>-</sup>CD45<sup>+</sup>CD11b<sup>+</sup>Ly6G<sup>++</sup>T1-Cy5<sup>-</sup> and (3) Ly6G<sup>low</sup>T1p = DAPI<sup>-</sup>CD45<sup>+</sup>CD11b<sup>+</sup>Ly6G<sup>low</sup>Ly6C<sup>low</sup>T1-Cy5<sup>+</sup>. After sorting, isolated cells were assessed for viability and purity. Isolated cell populations were processed for histochemistry (H&E staining, HMRI-Research Pathology Core), RNA isolation/transcriptome analysis and functional assays.

### Transcriptomic analysis

Cell populations isolated by flow cytometry sorting were processed with RNeasy Plus Micro Kit (Qiagen) for RNA isolation according to manufacturer's instructions. RNA quality and quantity were assessed by Bioanalyzer (RNA Core at Houston Methodist Research Institute) and samples were submitted to RNA sequencing (Novogene, Sacramento, CA). During sequencing a library preparation kit was used that is specifically suited to accommodate low amounts of input RNA.

### T cell suppression assay, IFN $\gamma$ ELISpot

In T cell suppression assays we used antigen-specific T-cell activation, and syngeneic T-cell/MDSC co-cultures. Specifically, T cells of TCR-transgenic OT-1 mice on C57 BL/6 background were co-cultured with MDSCs from MC38 tumor model, DO11.10-derived TCR transgenic T-cells on BALB/C background were used with MDSCs from CT26 model. T cells of spleen of TCR transgenic mouse (OT-1 on C57 BL/6 background for experiments with MC38 tumor model, DO11.10 on BALB/C background for CT26 model) were isolated using mouse T cell isolation kit (Stem Cell Technologies, Vancouver, Canada). Cells were labeled with 1  $\mu$ M CFSE following supplier-instructions (Cell Trace CFSE, Thermo Fisher Scientific, Waltham, MA). Antigen presenting cells were prepared from spleen by utilizing negative fraction of Thy1.2 T cell isolation procedure (Stem Cell Technologies, Vancouver, Canada). T cells and antigen presenting cells were mixed with SIINFEKL peptide (OVA 1, for OT-1 model) or OVA 2 for DO11.10 model at 10  $\mu$ g/ml and incubated with 2.5 fold excess (relative to T cell number) of MDSC populations for 72 h at 37°C. At end of culture period, cells were collected and stained for FACS with anti-CD3, anti-CD8a, anti-CD4, anti-PD1, anti-CD11b and DAPI, followed by addition of counting beads.

### IFN $\gamma$ ELISpot

Protocol was based on previously published approach (Nagaraj et al., 2010). Splenocytes of TCR transgenic mice (OT-1 on C57 BL/6 background for experiments with MC38 tumor model, DO11.10 on BALB/C background for CT26 model (Sinha et al., 2012)) were co-cultured with MDSC populations (ratio splenocytes: MDSC = 1:2.5) in presence of antigen (OVA1 for OT-1 and OVA2 for DO11.10, 10  $\mu$ g/ml) in T cell medium for 44 h. T cells were re-stimulated on ELISpot plates as follows: ELISpot plates (IP Sterile Clear Plates with Immobilon P membrane, MilliporeSigma, St. Louis, MO) were pre-treated and coated with anti-mouse IFN $\gamma$  capture antibody at 4°C overnight. Membrane was blocked with T cell medium. T cells were isolated from 44 h-co-cultures with MDSC subset (T cell isolation kit, Stem Cell Technologies), mixed with splenocytes of naïve mouse (ratio T cells:splenocytes = 1:4) and antigenic peptide (10  $\mu$ g/ml) and cultured for 20 h on ELISpot plates in T cell medium. To detect IFN $\gamma$ + spots as final step of the procedure, plates were treated with 0.01% Tween-20 in PBS and PBS, followed by 2 h incubation at room temperature with biotinylated IFN $\gamma$  detection antibody in assay diluent (BD Biosciences, San Jose, CA), washes, 30 min incubation with avidin-HRP in assay diluent, washes and final incubation with freshly prepared AEC substrate solution (BD Biosciences, San Jose, CA) for 20-30 min. Plates were extensively washed under running water, dried and submitted to spot counting using an ELISpot reader.

### Mass spectrometric identification of T1 aptamer binding partner

T1 aptamer was modified with ABAL moiety, i.e. attaching a linker coupled to phenyl-azide and biotin (ABAL moiety: MilliporeSigma, St. Louis, MO, T1-ABAL synthesis: IDT Technologies, Coralville, Iowa). This allowed for UV-crosslinking T1 aptamer to interacting proteins via phenyl-azide, and enrichment of T1 binding proteins on streptavidin-columns via biotin. Streptavidin-column enrichment of T1 binding proteins and mass spectrometric identification were carried out by Phenoswitch (Sherbrooke, Canada). We adopted the approach developed by (Vinkenborg et al., 2012). ABAL-T1 was incubated with target cells 30 min on ice, UV-crosslinked to interacting proteins via phenyl-azide (8000 U irradiation, UV-crosslinker, Hofer Instruments, Holliston, MA) and extensively washed to remove unbound aptamer. Control samples were obtained by pre-incubation with 50x excess of unlabeled T1, followed by the same processing. Remaining steps of column enrichment of T1 binding proteins from cell lysates and mass spectrometry analysis were carried out by Phenoswitch (Sherbrooke, Canada). Cells were lysed (50 mM Tris pH 8, 150 mM NaCl, 1% Triton, 1 mM EDTA). Biotin pulldown was performed using MagResyn Streptavidin magnetic beads overnight. The beads were washed with a harsh buffer (50 mM Tris pH 8, 350 mM NaCl, 1% Triton, 1 mM EDTA) to remove unspecific binding. After reduction and alkylation, proteins were digested on the bead with Trypsin/LysC overnight. Resulting peptides were purified by reversed phase SPE and analyzed by LC-MS. Data quantification: A publicly available ion library for human samples (Swath Atlas) was used in the

Peakview software (ABSciex) to quantify the proteins in sample, using 3 transition/peptide and 100 peptides/protein. A peptide was considered as adequately measured if the score computed by Peakview was superior to 1.5 and had an FDR < 5%. The sum of the AUC was corrected on the total signal for all the samples within the same group (Pre K and K).

### CRISPR KO

CRISPR KO was implemented with a two-step lentivirus-based system: First, K562 parental cells were lentivirally transduced with an expression construct for CAS9 and GFP (Wang et al., 2017). GFP<sup>+</sup> single cell-derived clones were generated (K562 CAS9). Clones with high CAS9 expression based on Western blots were used further. Second, K562 CAS9 cells were transduced with guide RNA targeting gene of interest (SDC-1 and Exostosin-1 (Ren et al., 2018), respectively). Lentiviral constructs (pLentiGuide-Puro) for the expression of guide RNA were prepared and verified by sequencing (GenScript Biotech, Piscataway, NJ). gRNA for SDC-1: 5' GAGACGTGGGAATAGCCGTC 3' (Fan et al., 2017); gRNA for Exostosin-1: 5' GTCTGGTTCCTCGTGGTCGC 3' (Ren et al., 2018). KO lines (transduced with constructs of gene-specific gRNA for SDC-1 or Exostosin-1), were purified by puromycin selection. KO was verified by flowcytometry and confocal microscopy, i.e. loss of syndecan-1 expression in SDC-1 KO line, and loss of heparan sulfate on cell surface of Exostosin-1 KO line, respectively. Cells were stained with anti-human syndecan-1 PE (clone DL101, Biolegend, San Diego, CA) or anti-heparin/heparan sulfate (MAB2040, MilliporeSigma, St. Louis, MO) followed by FITC-labeled anti-mouse IgG.

### Confocal microscopy

K562, a non-adherent cell line, and derivatives were all processed in suspension. After blocking in 200 ul PBS with 4% FBS they were stained with anti-human syndecan-1 (clone MI15, Biolegend), or anti-heparin/heparan sulfate (MAB2040, MilliporeSigma, St. Louis, MO) and incubated on ice with T1-Cy5 (200 nM) in aptamer binding buffer. Next, cells were stained with secondary AF488-labeled anti-mouse IgG, 4% PFA-fixed and DAPI-stained (0.5 ug/ml). Cells were applied to positively charged slides (Superfrost Plus Microscope slides, Thermo Fisher Scientific, Waltham, MA) by Cytospin (10,000-100,000 cells per slide, 8 min, 2000 rpm). Slides were evaluated and imaged on a confocal microscope Fluo View TM3000 (Olympus, Shinjuku, Japan) at 100x magnification.

## QUANTIFICATION AND STATISTICAL ANALYSIS

### Statistical analysis

GraphPad Prism version 6.01 (GraphPad Software, Inc, California, USA) and statistical functions in Excel were used. Difference between two values was evaluated with a two-tailed, unpaired Student's t-test. For correlation of flowcytometric parameters, each individual cell's parameter values were exported to Excel worksheet then correl function in Excel was applied to calculate R (Pearson correlation coefficient). In multiple comparisons of more than two experimental groups, 2way ANOVA Tukey's multiple comparisons test was used. Gene set enrichment analysis (GSEA): GSEA software, a joint project of UC San Diego and Broad Institute was applied following instructions on the website <https://www.gsea-msigdb.org/gsea/index.jsp>.